Article

TRANSPARENT PROCESS OPEN ACCESS

THE EMBO JOURNAL

Regulators of complement activity mediate inhibitory mechanisms through a common C3b-binding mode

Federico Forneris[1,†], Jin Wu[1], Xiaoguang Xue[1], Daniel Ricklin[2], Zhuoer Lin[2], Georgia Sfyroera[2], Apostolia Tzekou[2], Elena Volokhina[3], Joke CM Granneman[1], Richard Hauhart[4], Paula Bertram[4], M Kathryn Liszewski[4], John P Atkinson[4], John D Lambris[2] & Piet Gros[1,*]

Abstract

Regulators of complement activation (RCA) inhibit complement-induced immune responses on healthy host tissues. We present crystal structures of human RCA (MCP, DAF, and CR1) and a small-pox virus homolog (SPICE) bound to complement component C3b. Our structural data reveal that up to four consecutive homologous CCP domains (i–iv), responsible for inhibition, bind in the same orientation and extended arrangement at a shared binding platform on C3b. Large sequence variations in CCP domains explain the diverse C3b-binding patterns, with limited or no contribution of some individual domains, while all regulators show extensive contacts with C3b for the domains at the third site. A variation of ~100° rotation around the longitudinal axis is observed for domains binding at the fourth site on C3b, without affecting the overall binding mode. The data suggest a common evolutionary origin for both inhibitory mechanisms, called decay acceleration and cofactor activity, with variable C3b binding through domains at sites ii, iii, and iv, and provide a framework for understanding RCA disease-related mutations and immune evasion.

Keywords complement; regulators of complement activity; cofactor activity; decay-accelerating activity; immune evasion
Subject Categories Immunology; Structural Biology
DOI 10.15252/embj.201593673 | Received 11 December 2015 | Revised 19 February 2016 | Accepted 29 February 2016 | Published online 24 March 2016
The EMBO Journal (2016) 35: 1133–1149

Introduction

The complement system is an important arm of the humoral immune system in mammals (Sjoberg *et al*, 2009; Ricklin *et al*, 2010; Merle *et al*, 2015a,b). Activation of the complement leads to C3b opsonization of targeted cells and particles inducing killing and clearance of the target. To protect host cells and tissues from inadvertent complement activation, mammals express complement regulators, such as factor H (FH), complement receptor 1 (CR1, CD35), membrane-cofactor protein (MCP, CD46), and decay-accelerating factor (DAF, CD55; Zipfel & Skerka, 2009; Merle *et al*, 2015a). These regulator proteins stop C3b opsonization by breaking down the C3 convertases. Lack of protection, due to familial mutations in the complement genes (Liszewski & Atkinson, 2015a; Martinez-Barricarte *et al*, 2015) or the presence of autoantibodies against regulators (Luzzatto & Gianfaldoni, 2006; Dragon-Durey *et al*, 2010), has been linked to, for example, atypical hemolytic uremic syndrome (aHUS) and C3 glomerulopathies (C3G) in kidneys and age-related macular degeneration (AMD) in eyes. Moreover, conditions of chronic and acute inflammations, as in rheumatoid arthritis, strokes, and heart attacks, become aggravated by complement activation against the disturbed tissue (Sjoberg *et al*, 2009; Merle *et al*, 2015b). These pathological conditions underscore the importance of balancing complement activation and regulation (Ricklin & Lambris, 2013a).

Proteins of the "regulators of complement activation" (RCA) gene cluster consist of strings of consecutive complement control protein (CCP) domains of ~60–70 amino-acid residues (Kirkitadze & Barlow, 2001). Complement regulators CR1, MCP, and DAF are expressed on cell membranes, where they provide immediate protection to host cells. The soluble regulator FH stops complement activation in the fluid phase and discriminates "self" from "non-self" cells and matrix material by binding host molecular patterns (Clark *et al*, 2013). The protective function can be attributed to 3–4 consecutive CCP domains (Kirkitadze & Barlow, 2001; Zipfel & Skerka, 2009; Merle *et al*, 2015a), which may act through two inhibitory mechanisms. DAF, CR1, and FH have so-called decay-accelerating activity. Decay acceleration enhances the irreversible

1 Crystal and Structural Chemistry, Bijvoet Center for Biomolecular Research, Department of Chemistry, Faculty of Science, Utrecht University, Utrecht, The Netherlands
2 Department of Pathology & Laboratory Medicine, University of Pennsylvania, Philadelphia, PA, USA
3 Department of Pediatric Nephrology (830), Radboud University Medical Center, Nijmegen, The Netherlands
4 Department of Medicine, Division of Rheumatology, Washington University School of Medicine, St. Louis, MO, USA
*Corresponding author. Tel: +31 30 253 3127; E-mail: p.gros@uu.nl
†Present address: The Armenise-Harvard Laboratory of Structural Biology, Department of Biology and Biotechnology, University of Pavia, Pavia, Italy

dissociation of protease fragments from C3 convertases, either C4b2a or C3bBb (Nicholson-Weller & Wang, 1994; Hourcade *et al*, 1999). Linked to this first activity, the regulators also block the binding of proenzymes and prevent the formation of new convertases. MCP, CR1, and FH exert cofactor activity. By binding to C3b or C4b, these regulators provide a binding platform for the protease factor I (FI). Bound FI cleaves C3b and C4b to yield fragments that cannot form convertases. Viruses and bacteria utilize these host protection mechanisms to avoid complement response. While certain bacteria express surface-bound proteins that bind host FH to provide protection (Zipfel *et al*, 2013; Merle *et al*, 2015b; Schmidt *et al*, 2015), orthopox and herpes viruses encode their own protection proteins, which structurally and functionally mimic host regulators (Ahmad *et al*, 2007; Ojha *et al*, 2014). Variola virus "smallpox inhibitor of complement enzymes" (SPICE) consists of four CCP domains and exhibits both decay-accelerating and cofactor activities (Rosengard *et al*, 2002) and is 40% identical in amino-acid sequence to human MCP.

A structural basis of regulator binding to C3b was provided by crystal structures of C3b in complex with FH domains CCP1–4 (Wu *et al*, 2009) and C3d in complex with FH CCP19–20 (Kajander *et al*, 2011; Morgan *et al*, 2011). The structure of C3b-FH CCP1–4 shows C3b in its characteristic arrangement of a key-ring-shaped core consisting of 6 macroglobulin domains (MG1–6) connected by a linker domain, two domains (MG7–8) on top of the key ring that connect to an arm formed by a "complement C1r/C1s, UEGF, BMP1" (CUB) domain and thioester-containing domain (TED); and a C-terminal C345c (CTC) domain at the top of C3b (Janssen *et al*, 2006; Wiesmann *et al*, 2006; see Fig 1). The FH CCP1–4 binding site spans C3b from the α′ N-terminal (α'NT) region bound to MG7, through MG6, MG2, and CUB, down to MG1 and TED. The C-terminal CCP19–20 domains of FH bind at a distinct binding site provided by the TED domain. Taken together, "mini-FH" chimeras consisting of the CCP1–4 and 19–20 showed strong decay-accelerating and cofactor activities, similar to those of full-length FH (Hebecker *et al*, 2013; Schmidt *et al*, 2013). Structure comparison of C3b-FH CCP1–4 and the C3 convertase (C3bBb) in complex with SCIN (Rooijakkers *et al*, 2009) suggested that FH displaces Bb by steric hindrance upon binding to C3b, thereby exerting its decay-acceleration activity. Furthermore, crystal structures of FB in complex with C3b or the homologous cobra-venom factor (CVF; Janssen *et al*, 2009; Forneris *et al*, 2010) revealed overlapping binding sites for the CCP1–2 domains of FB and the CCP1–2 domains of FH, which explains why binding of FH to C3b blocks convertase formation. In the case of cofactor activity, regulator binding to C3b provides a binding platform for the protease FI. Roversi *et al* presented a crystal structure of FI (Roversi *et al*, 2011) and suggested that FI possibly binds at a niche formed by the regulator domains CCP1–3 of FH and the CTC domain of C3b, providing a potential explanation for the regulator role in cofactor activity of FH.

Regulators vary in activity and C3b- and C4b-binding behavior, even though all regulators consist of strings of homologous CCP domains (Kirkitadze & Barlow, 2001; Ahmad *et al*, 2007; Harris *et al*, 2007; Zipfel & Skerka, 2009; Merle *et al*, 2015a). Both MCP and DAF require their CCP3–4 for binding to C3b (Liszewski *et al*, 2000; Harris *et al*, 2007) and CCP2–4 for cofactor activity (Liszewski *et al*, 2000; Riley *et al*, 2002) and decay-accelerating activity, respectively (Harris *et al*, 2007). However, their CCP2–4 domains map to CCP2–4 and CCP1–3 of FH, respectively (McLure *et al*, 2004). CR1 bears three clusters of CCP domains displaying differential C3b/C4b binding and associated regulatory activities. The CCP1–3 domain binds weakly to C3b and strongly to C4b (Krych *et al*, 1991) and predominantly shows decay acceleration in both classical and alternative pathways (Krych-Goldberg *et al*, 1999), whereas the two domain clusters CCP8–10 and CCP15–17, identical in sequence with the exception of four amino acids, bind strongly to both C3b and C4b (Krych *et al*, 1994) and display mostly cofactor activity (Krych *et al*, 1994, 1998). Furthermore, FH and CR1 binding to C3b depends on interactions with the α'NT region, whereas MCP does not (Lambris *et al*, 1996; Krych *et al*, 1998; Oran & Isenman, 1999; Makou *et al*, 2013). Extensive mutagenesis data for MCP (Liszewski *et al*, 2000) show that C3b binding of domain CCP4 of MCP is incompatible with the observed arrangement of the equivalent domain in C3b-FH CCP1–4 complex (Wu *et al*, 2009). Various mutations of regulators linked to aHUS, C3G, and AMD have been reported (Weisman *et al*, 1990; Zipfel & Skerka, 2009; Rodriguez *et al*, 2014; Liszewski & Atkinson, 2015b; Schramm *et al*, 2015). These mutations identify multiple sites on the surface of C3b, FH, MCP, and CR1 responsible for effective complement regulation. The available structural data from the C3b-FH (CCP1–4; Wu *et al*, 2009) and C3d-FH (CCP19–20; Kajander *et al*, 2011; Morgan *et al*, 2011) complexes and the structures of isolated regulators (Smith *et al*, 2002; Uhrinova *et al*, 2003; Williams *et al*, 2003; Lukacik *et al*, 2004; Persson *et al*, 2010) provided initial guidance for structural mapping of these mutations. However, the differences in the sequences and structural orientations of the various CCP domains of the regulators did not provide an unambiguous molecular explanation for several disease-related mutations (Dragon-Durey & Fremeaux-Bacchi, 2005; Rodriguez *et al*, 2014; Liszewski & Atkinson, 2015b; Martinez-Barricarte *et al*, 2015; Schramm *et al*, 2015). In addition, Gropp *et al* (2011) indicated β2-glycoprotein I, which consists of five CCP domains, to act as a complement regulator (Gropp *et al*, 2011). To provide a structural basis for binding of the regulators and their activities, we determined the crystal structures of human DAF domains CCP2–4, MCP CCP1–4, CR1 CCP15–17, and the variola virus SPICE (full-length CCP1–4) in complex with human C3b. In addition, we report the structure of "free" C3b at 2.8-Å resolution, thereby improving the resolution of an earlier report (Janssen *et al*, 2006). These data indicate a common binding site on C3b for the regulators and suggest a common structural origin for the complement-inhibitory activities by the "regulators of complement activation (RCA)".

Results and Discussion

Structural data

We determined the crystal structures of C3b-MCP (CCP1–4), C3b-SPICE (CCP1–4), C3b-CR1 (CCP15–17), and C3b-DAF (CCP2–4) to 2.4, 2.5, 3.3, and 4.2-Å resolution, respectively (Table 1 and Fig 1A). Previously, we reported the crystal structure of C3b-FH (CCP1–4) at 2.7-Å resolution (Wu *et al*, 2009). For these fragments, we observed K_D's of 0.35 μM for MCP (CCP1–4), 1.3 μM for SPICE (CCP1–4), 1.9 μM for CR1 (CCP15–17), 6.1 μM for DAF (CCP1–4),

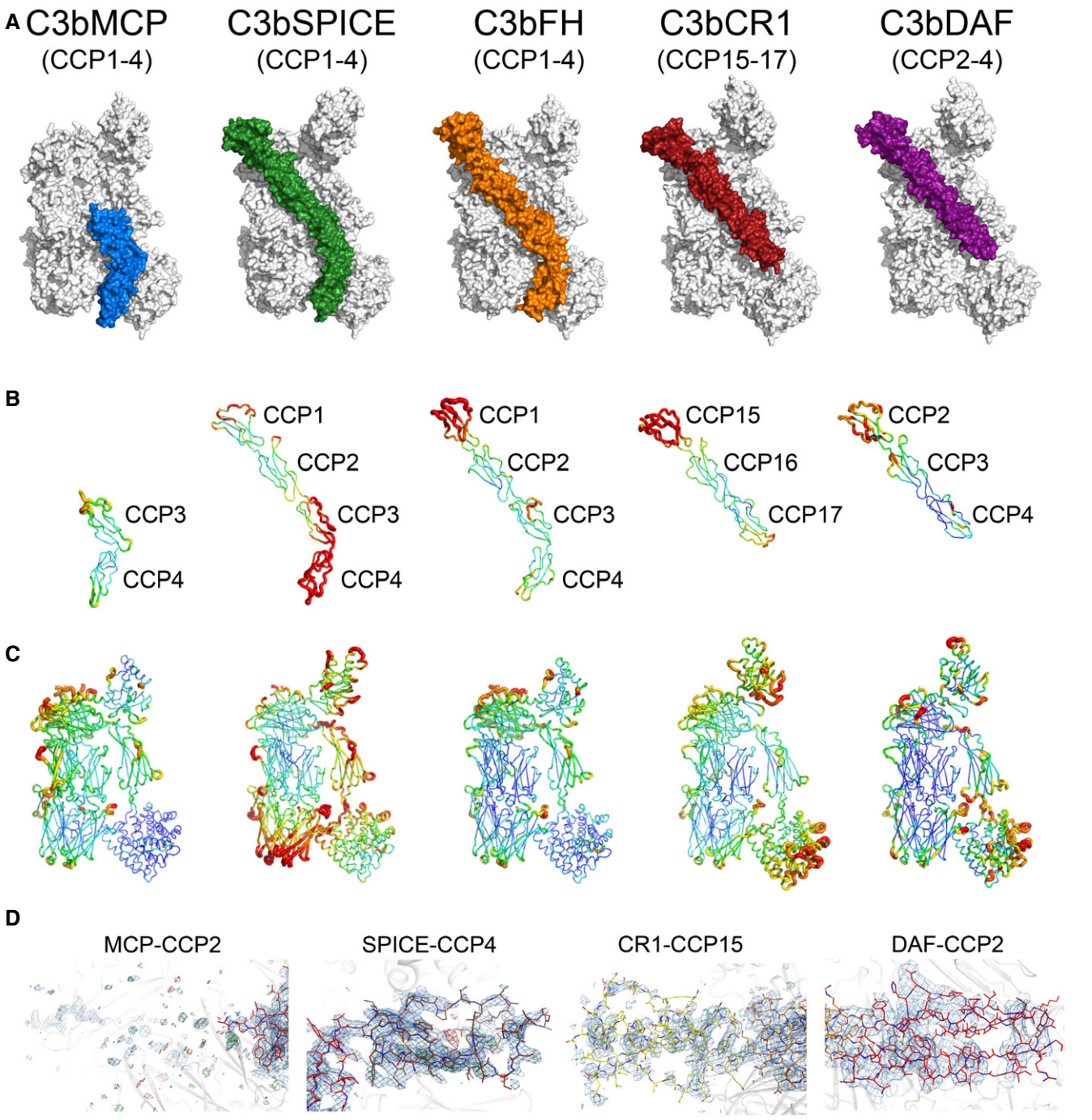

Figure 1. Structural overview of C3b-regulator complexes.

A From left to right, surface representation of the three-dimensional structures of C3b-MCP (CCP1–4) (blue), C3b-SPICE (CCP1–4) (green), C3b-FH (CCP1–4) (orange), C3b-CR1 (CCP15–17) (dark red), C3b-DAF (CCP2–4) (purple).

B Cartoon representation of the five regulators. The width of the cartoon is proportional to the B-factors observed in the structural data. The B-factor coloring (from blue to red) is in relative scale according to the resolution of the crystal structures.

C Cartoon representation of the five C3b molecules in the C3b-regulator complexes. Coloring and style as in (B).

D Highlight of electron density maps ($2F_o$-F_c, blue, contour level 1.2σ; F_o-F_c, green and red, contour level 3σ and −3σ, resp.) for the regions of the C3b-regulator complexes showing flexibility. From left to right: the putative site for MCP CCP2, SPICE CCP4, CR1 CCP15, and DAF CCP2.

and 7.2 μM for FH (CCP1–4); see Fig EV1. Furthermore, initial crystallization trials of C3b-CR1 (CCP15–17) and C3b-β2GPI yielded crystals containing only C3b. One of these crystals was used to collect a C3b data set up to 2.8-Å resolution, superseding the C3b structure at low resolution currently available in the PDB (Janssen *et al*, 2006).

Table 1. Diffraction, data collection, and refinement statistics.

	C3b-DAF (CCP2–4)	C3b-CR1 (CCP15–17)	C3b-MCP (CCP1–4)[a]	C3b-SPICE (CCP1–4)	C3b
Data collection[b]					
Space group	$P2_122_1$	P1	$P2_122_1$	P1	$P2_1$
Cell parameters	a = 117.4 Å α = 90.0° b = 142.4 Å β = 90.0° c = 323.7 Å γ = 90.0°	a = 104.3 Å α = 82.7° b = 113.7 Å β = 71.8° c = 138.5 Å γ = 80.9°	a = 82.8 Å α = 90.0° b = 130.6 Å β = 90.0° c = 233.8 Å γ = 90.0°	a = 68.9 Å α = 75.0° b = 83.3 Å β = 76.2° c = 127.4 Å γ = 68.5°	a = 57.6 Å α = 90.0° b = 136.5 Å β = 96.1° c = 140.9 Å γ = 90.0°
X-ray source	ESRF ID14 EH4	ESRF ID23 EH1	ESRF ID29	ESRF ID14 EH4	ESRF ID14 EH4
Data processing software	iMOSFLM/SCALA	iMOSFLM/SCALA	iMOSFLM/AIMLESS	XDS/AIMLESS	iMOSFLM/AIMLESS
Wavelength (Å)	0.975	0.873	0.933	0.939	0.939
Resolution (Å)	117.83–4.20 (4.43–4.20)	60.15–3.30 (3.48–3.30)	69.95–2.40 (2.44–2.40)	47.80–2.50 (2.55–2.50)	70.07–280 (2.89–2.80)
Molecules per ASU	2	2	1	1	1
Unique reflections	39,033 (5,369)	88,061 (12,811)	98,854 (4,722)	84,531 (4,525)	109,359 (9,703)
Redundancy	4.1 (3.9)	1.9 (1.9)	3.8 (2.9)	2.0 (1.9)	2.1 (2.1)
I/σ(I)	6.3 (2.3)	3.8 (1.4)	6.8 (2.0)	4.3 (1.0)	9.4 (1.5)
Completeness (%)	96.5 (92.6)	98.4 (98.2)	99.0 (96.2)	97.2 (96.3)	96.8 (98.3)
CC1/2	n.d.	n.d.	0.988 (0.693)	0.963 (0.527)	0.954 (0.685)
R_{meas}[c]	0.175 (0.673)	0.225 (0.878)	0.116 (0.583)	0.128 (0.774)	0.122 (1.098)
Refinement					
R_{work}/R_{free}	0.258/0.296	0.250/0.291	0.188/0.219	0.198/0.229	0.229/0.268
Average B-factors (Å)^2					
Overall	192	143	67	80	107
C3b only	189	137	67	78	107
Regulator only	218	179	73	100	N/A
Number of atoms	27,275	27,406	13,810	14,478	12,150
Protein	27,275	27,378	13,123	14,036	12,122
Ligands (including glycans)	0	28	195	235	28
Waters	0	0	492	207	0
R.M.S. deviations					
Bond lengths (Å)	0.005	0.003	0.005	0.004	0.003
Bond angles (°)	1.04	0.83	0.85	0.88	0.65
Ramachandran statistics					
Favored (%)	93	96	97	96	96
Allowed (%)	6	4	2	3	4
Disallowed (%)	1	0	1	1	0

[a]In the crystal structure of C3bMCP (CCP1–4), only CCP domains 3 and 4 could be modeled.
[b]Values in parentheses are for reflections in the highest resolution shell.
[c]$R_{meas} = \Sigma_{hkl} \{n/[n-1]\}^{1/2} \times \Sigma_i | I - \langle I \rangle | / \Sigma_{hkl} \Sigma_i I$, where I is the observed intensity for a reflection and $\langle I \rangle$ is the average intensity of symmetry-related observations of a unique reflection.

C3b-regulator arrangements

The regulators bound to C3b show extended arrangements of their CCP domains, while C3b displays its characteristic organization of MG1–8, linker, CUB, TED, and CTC domains (Janssen *et al*, 2006, 2005; Wiesmann *et al*, 2006; Fig 2A). The extended CCP arrangements are in agreement with the structures of unbound regulators and regulator fragments (Smith *et al*, 2002; Uhrinova *et al*, 2003; Williams *et al*, 2003; Lukacik *et al*, 2004; Persson *et al*, 2010; Appendix Fig S3). Overall, the regulators bind C3b at the same site, formed by the α'NT region and domains MG7, MG6, CUB, MG2, MG1, and TED (top to bottom as shown in Fig 2A), similar to that observed in the complex of C3b with FH CCP1–4 (Wu *et al*, 2009). The C3b-regulator contact interfaces extend over a length of up to 130 Å burying surface areas up to 2,300 Å^2 (see Fig 2 for details).

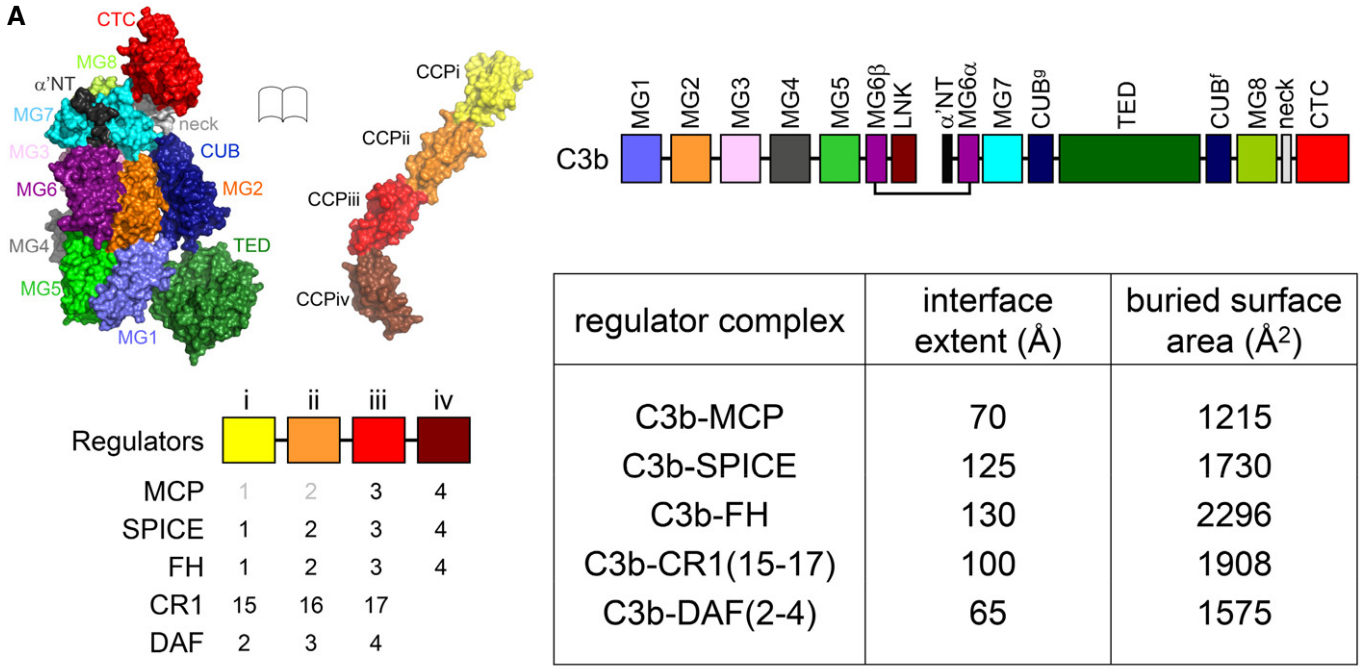

regulator complex	interface extent (Å)	buried surface area (Å^2)
C3b-MCP	70	1215
C3b-SPICE	125	1730
C3b-FH	130	2296
C3b-CR1(15-17)	100	1908
C3b-DAF(2-4)	65	1575

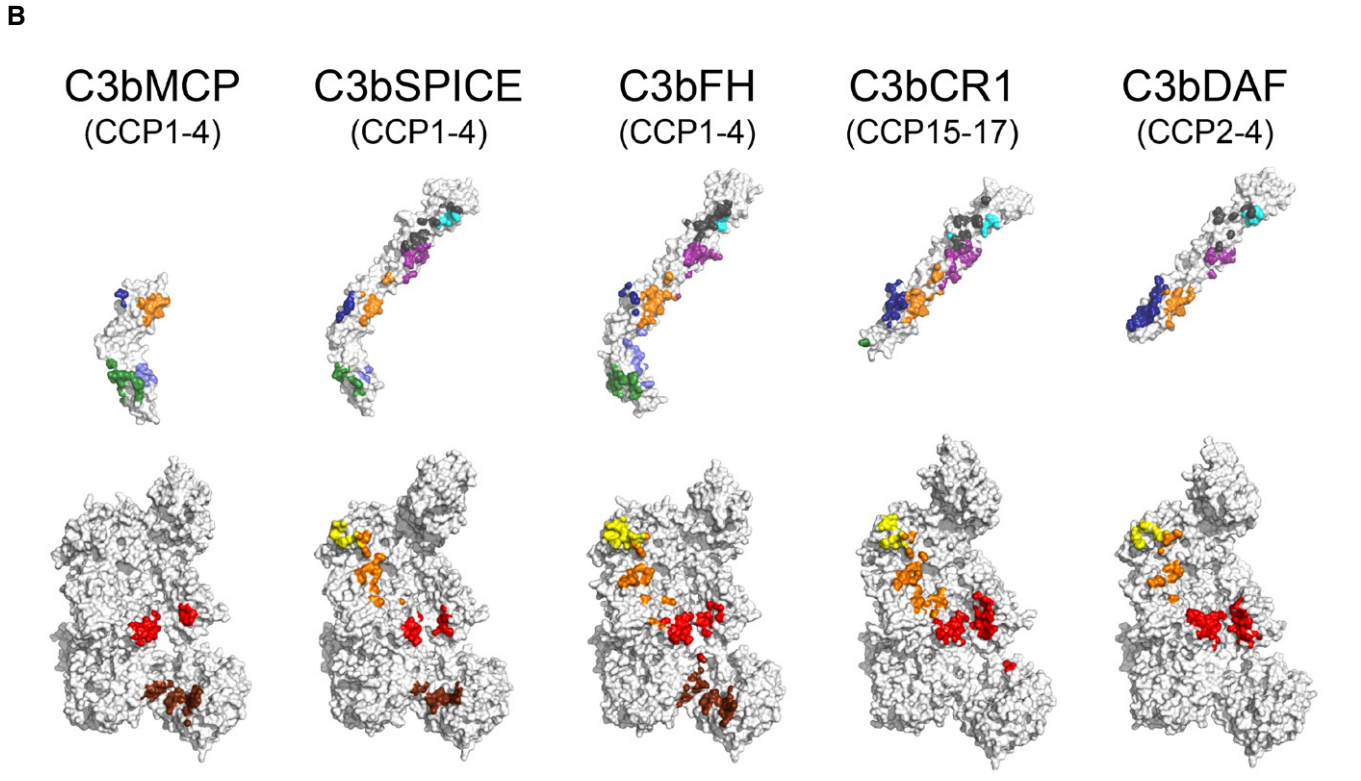

Figure 2. Domain organization in the C3b-regulator complexes and molecular interactions.

A "Open-book" surface representation of C3b and regulator molecules, highlighting their domain organizations using different colors as shown in the neighboring schemes. Domains in complement regulators are labeled using domain numbering from CCPi to CCPiv based on their contact sites on C3b. The corresponding CCP domains in each regulator described in this work are shown in the bottom-left scheme. Domains CCP1–2 of MCP are shown in shaded gray because they are not involved in C3b binding. The table reports the extent of the regulator contact surface on C3b and the associated buried surface area.

B Opened view of the molecular footprint of the regulator-C3b interaction (as shown in Fig 2A), highlighting the C3b domains on the regulator surface (top) and the regulator domains on C3b (bottom).

C3b-MCP differs markedly from C3b-FH CCP1–4 in two aspects. First, in C3b-MCP, only CCP3–4 makes contact with C3b. No density and non-interpretable density were observed for CCP1 and CCP2, respectively (Fig 1D), whereas the density was well resolved for the CCP3 and CCP4 domains of MCP (Appendix Fig S1). These observations are in agreement with biochemical data that CCP1 and CCP2 of MCP do not contribute to C3b binding (Adams *et al*, 1991). Second, the orientation of MCP CCP4 differs markedly from FH CCP4. Though MCP CCP4 domain binds at the same site to C3b, it is rotated by ~100° around the long axis of the domain compared to CCP4 of FH in C3b-FH (Fig 3A and B, Appendix Fig S4A). Figure 3C shows that mutagenesis data on CCP4 of MCP (Liszewski *et al*, 2000) is in full accordance with the observed domain orientation in the crystal structure. The competitive binding of the GB24 antibody to MCP, identified by mutagenesis around residues Phe230 and Phe242, further supports the observed MCP interaction site (Liszewski *et al*, 2000). The CCP4 domain of SPICE binds C3b in the same orientation as MCP CCP4, although the electron density for SPICE CCP4 was weak, indicating disorder and suggesting weak local interactions (Fig 1D). Limited contribution by SPICE CCP4 to C3b binding is supported by improved binding of vaccinia virus complement control protein (VCP) CCP1–3 fused to MCP CCP4 (Ahmad *et al*, 2010). Putatively, FH may be considered deviant from MCP and SPICE. FH may have evolved differently due to its subsequent domains that function in specific host-surface recognition (Clark *et al*, 2013).

Most C3b-regulator contacts involve the central CCP domains, that is, MCP CCP3–4, SPICE CCP2, FH CCP2–4, CR1 CCP16–17, and DAF CCP3–4 (Table 2), which correspond with areas of low B-factors (Fig 1B and C). The N-terminal domains, CCP1 of FH, CCP15 of CR1, and CCP2 of DAF, make only minor contacts to α'NT and MG7 at the C-terminal "bottom" side. These domains point outwards from the complexes and show variable orientations. The non-crystallographic symmetry copies of DAF CCP2 differ by 17°, resulting in a ~20 Å displacement, consistent with flexibility at the CCP2-CCP3 hinge of DAF (Appendix Fig S4A; Uhrinova *et al*, 2003). Overall, SPICE differs from the other regulators with low B-factors for CCP1–2 and high B-factors for the bottom side of CCP3 and the complete CCP4 domain (Fig 1B). Crystal contacts of SPICE CCP1 contribute to the local packing resulting in lower B-factors (Appendix Fig S2B). SPICE CCP3–4 domains pack against C3b-like CCP3–CCP4 of MCP (Fig 3A and B); however, these interactions appear to be weaker and the interactions with C3b are dominated by contacts through domains CCP1–2 of SPICE. The C-terminal CCP4 domains of MCP and FH interact extensively with C3b (though MCP and FH use distinct interaction faces of CCP4 in binding to C3b). For MCP, all contacts with C3b involve CCP3–4 only (Table 2, Fig EV2). Thus, marked differences in C3b-regulator contacts and CCP order–disorder are observed, which in part reflect the differences in interactions made by the CCP domains for binding to C3b.

C3b structural variations

The C3b structures in all regulator complexes display the typical domain organization of C3b (Appendix Fig S4B). Notably, CUB-TED and CTC show variable positioning with respect to the main body of C3b. The characteristic β-ring of C3b (Fig 2A) can be divided into a bottom (MG1, 4–5) and top part (MG2–3, 6) with flexibility for the bottom part that is higher as observed in C3b-SPICE and the unbound C3b at 2.8-Å resolution compared to that observed in the other presented structures (Fig 1C, Appendix Fig S4D). Variations in CUB-TED and CTC positions and between the β-ring top and bottom parts were previously observed in C3bB, C3bBD (Forneris *et al*, 2010) and the SCIN-stabilized C3bBb convertase (Rooijakkers *et al*, 2009), in its bovine ortholog (Fredslund *et al*, 2006), and in paralogs such as alpha-2-macroglobulin (Marrero *et al*, 2012), C5 (Fredslund *et al*, 2008), and the C5b-C6 complex (Aleshin *et al*, 2012; Hadders *et al*, 2012).

The CTC domain of C3b adopts different orientations with the "neck" that links CTC to the MG core found in two distinct conformations. This neck region (residues 1,496–1,517) connects CTC to MG8 through the main chain and participates in three disulfide bonds; one internal (Cys1506–Cys1511) and one each connecting to MG7 (Cys873–Cys1513) and to the CTC domain (Cys1518–Cys1590; Appendix Fig S5). During conversion from C3 to C3b, this region undergoes a complete change of its secondary structure. In C3, residues 1,507- to 1,517-fold into a α-helix (Janssen *et al*, 2005; Fredslund *et al*, 2006). In unbound C3b, the internal disulfide bond connects two short β-strands (respectively, 1,503–1,508 and 1,509–1,515) that fold into a short β-turn-β configuration (Janssen *et al*, 2006; Wiesmann et al, 2006). This conformational change positions CTC in a more upward orientation, while the MG7-MG8-CUB arrangement does not change (Appendix Fig S5). In the structures of C3b-SPICE, C3b-CR1, and C3b-DAF, the neck region adopts the β-turn-β configuration (Appendix Fig S5), as for all reported C3b structures except C3b-FH CCP1–4 (Janssen *et al*, 2006; Wiesmann *et al*, 2006; Katschke *et al*, 2009; Rooijakkers *et al*, 2009; Wu *et al*, 2009; Forneris *et al*, 2010; Garcia *et al*, 2010). The same conformational change is observed for conversion from C4 to C4b (Kidmose *et al*, 2012; Mortensen *et al*, 2015) and from C5 to C5b (Fredslund *et al*, 2008; Aleshin *et al*, 2012; Hadders *et al*, 2012). In the C3b-MCP and C3b-FH structures, the neck region adopts the α-helical configuration and is almost identical to that observed in C3. In these structures, the CTC shows a pronounced downward orientation (Fig EV3A). In this down position, a protruding loop of CTC (residues 1,585–1,600) contacts CUB, with aromatic residues Phe1558 and Trp1612 of CTC surrounding CUB residue Pro972 (Appendix Fig S6B). This arrangement is similar to the CTC-CUB contact observed in native C3. In C3b, the CTC loop docks on the β-hairpin conformation of the neck region through π-π stacking of the aromatic residues with Arg1507 and Arg1512 (Appendix Fig S6B). Since MCP, CR1 (CCP15–17), and FH have strong cofactor activity, the observed arrangements of CTC in C3bFH (CCP1–4) and C3bMCP (CCP1–4) may possibly reflect a preferred conformational arrangement for binding of FI; however, this arrangement is not observed for C3bCR1 (CCP15–17).

Besides the variations in C3b CTC positions (Fig EV3A), we observe differences in the placement of CUB and TED domains (Fig EV3B–D). The series of structures can be separated into two sets that differ by ~6–9 Å in CUB position as shown for residues 1,311–1,317 (Fig EV3C and D). Structures of C3b-DAF (CCP2–4) and C3b-CR1 (CCP15–17) show CUB-TED, with high B-factors, positioned in a downward orientation, while C3b-FH, C3b-MCP, and C3b-SPICE have CUB-TED in an upward position (Fig EV3B). The largest distinction between these two sets of structures is the

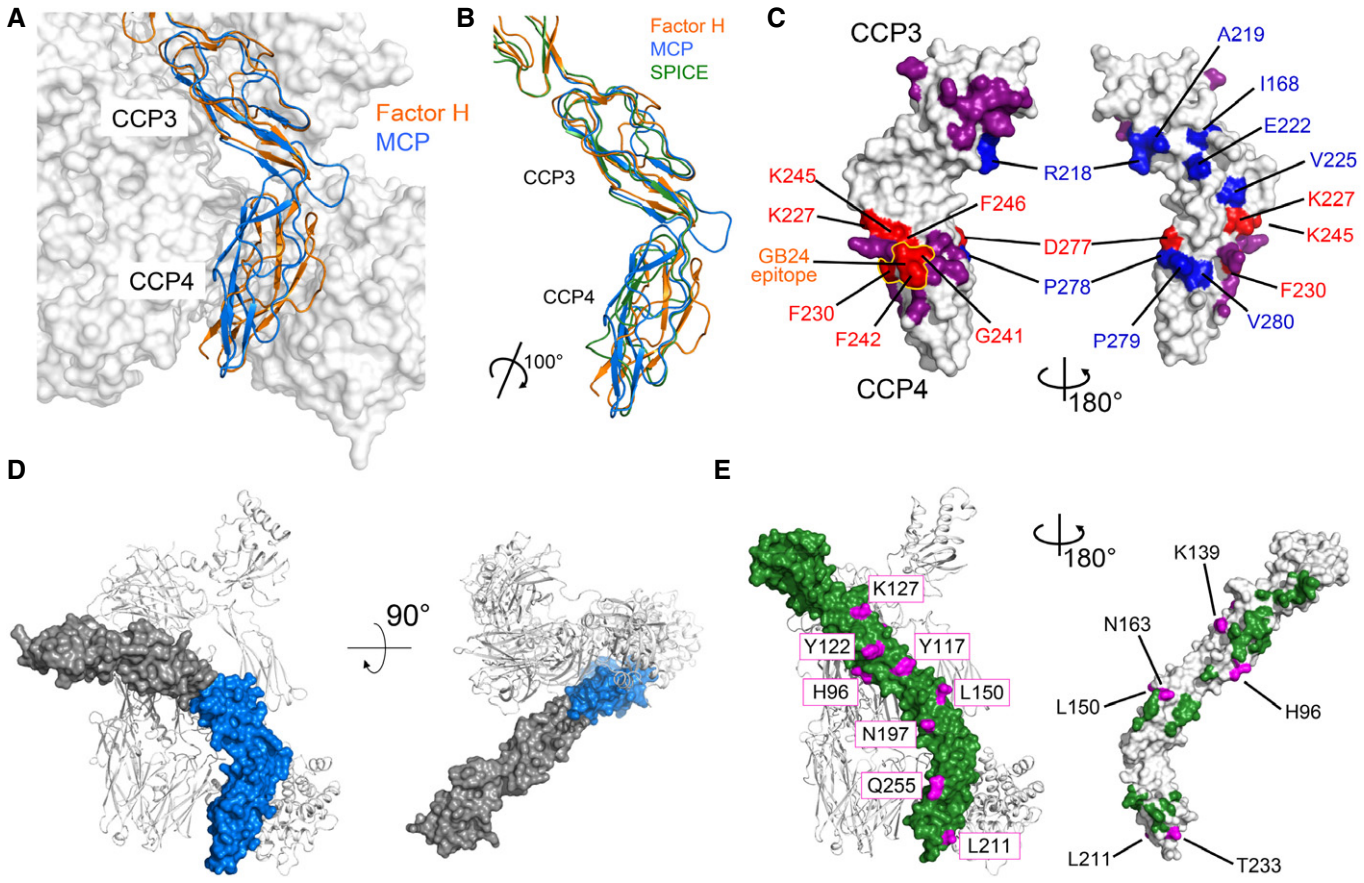

Figure 3. Molecular features of C3b-bound MCP and SPICE and comparison with C3b-FH.

A Superposition of MCP and FH domains CCP3–4 (shown as blue and orange cartoons, respectively) on the surface of C3b.

B Cartoon representation of the superposition of domains CCP3–4 of MCP (blue), FH (orange), and SPICE (green). Despite the strong structural similarity and the conserved angle between domains CCP3 and CCP4, MCP and SPICE show a rotation of approximately 100° in the position of CCP4 compared to FH.

C The reported mutagenesis data on MCP CCP3 and CCP4 (data from Liszewski *et al*, 2000) are consistent with the crystal structure. Shown are two orientations of the surface of MCP CCP3–4 as in the crystal structure of the C3b-MCP complex, highlighting the contact sites with the C3b platform (purple), the MCP mutations identified as critical for C3b binding (red) and those not affecting the interaction (blue). The GB24 antibody epitope is shown as yellow contour on the MCP surface.

D Model of the putative positioning of the flexible CCP1–2 domains of MCP. The model has been generated by superposing the structure of CCP1–4 of MCP from PDB 3O8E (Persson *et al*, 2010) onto the structure of the C3b-MCP (CCP1–4) complex. CCP1–2 domains of MCP, not visible in the C3b-MCP (CCP1–4) structure, are shown in gray.

E Highlight of the primary sequence differences between SPICE and VCP. The 11 mutations distinguishing the two viral regulators are shown on the surface of SPICE in purple. The contact surface of C3b on the regulator in the C3b-SPICE (CCP1–4) complex is shown in green on the right panel.

presence of a CCP domain binding to the MG1-TED site on C3b. With CUB-TED in the up position, more interactions between CUB and MG2 domains are observed forming a more tightly packed concave interface for interactions with the regulators (Fig EV3B–D). Additional hydrogen-bonding and salt-bridge interactions between these two domains involve the side chains of Arg979 with main chain carbonyl of Leu198, Arg937 with Glu226, Lys930 with Glu197, a proximate interaction (not forming hydrogen bonds in the structures) between Ser1315 and Gln177, and the main chain nitrogen of Leu1319 with the carbonyl of Pro174 of CUB and MG2, respectively (Appendix Fig S6A). Moreover, the upward orientation of CUB-TED facilitates the possible interactions with loop 1,607–1,622 of CTC. However, both up and down positions are observed in the two structures of (unbound) C3b and that of other C3b complexes (Janssen *et al*, 2006; Wiesmann *et al*, 2006; Katschke *et al*, 2009; Rooijakkers *et al*, 2009; Wu *et al*, 2009; Forneris *et al*, 2010; Garcia *et al*, 2010). This indicates that the energy difference between the two forms is small. The CUB-TED domains in the structure obtained at 2.8-Å resolution (reported here) are better packed (as judged by the B-factors and crystal contacts) and are placed in the up position. In the previously reported structure at 4-Å resolution (Janssen *et al*, 2006), these domains are in the down position with higher B-factors. Overall, the ~6–9 Å upward movement of CUB-TED observed for FH, MCP, and SPICE is likely induced by concerted bridging contacts between MG2 and CUB with the C-terminal part of CCP3 and contacts between the N-terminal part of CCP4 with TED. Together, these contacts result in a rearrangement of C3b domains MG2, CUB, and TED that has recently been indicated as critical for the strong cofactor activity of these regulators (Gautam *et al*, 2015).

Table 2. Summary of interactions details between C3b and regulators, divided by CCP domain[a].

	C3b-MCP (CCP1–4)	C3b-SPICE (CCP1–4)	C3b-FH (CCP1–4)	C3b-CR1 (CCP15–17)[b]	C3b-DAF (CCP2–4)[b]
Buried surface area (Å^b)[c]	CCP1: 0	CCP1: 311	CCP1: 419	CCP15: 284	CCP2: 230
	CCP2: 0	CCP2: 533	CCP2: 537	CCP16: 802	CCP3: 303
	CCP3: 443	CCP3: 374	CCP3: 643	CCP17: 865	CCP4: 843
	CCP4: 774	CCP4: 522	CCP4: 741		
	Total: 1217	Total: 1740	Total: 2340	Total: 1951	Total: 1376
Number of contacting amino acids	CCP1: 0	CCP1: 40	CCP1: 55	CCP15: 34	CCP2: 13
	CCP2: 0	CCP2: 70	CCP2: 61	CCP16: 83	CCP3: 36
	CCP3: 53	CCP3: 51	CCP3: 68	CCP17: 98	CCP4: 95
	CCP4: 88	CCP4: 58	CCP4: 80		
	Total: 141	Total: 219	Total: 264	Total: 215	Total: 144
Number of electrostatic contacts[d]	CCP1: 0	CCP1: 2	CCP1: 7	CCP15: 2	CCP2: 1
	CCP2: 0	CCP2: 9	CCP2: 2	CCP16: 7	CCP3: 1
	CCP3: 8	CCP3: 3	CCP3: 11	CCP17: 12	CCP4: 15
	CCP4: 16	CCP4: 6	CCP4: 9		
	Total: 24	Total: 20	Total: 29	Total: 21	Total: 17
Number of strong hydrophobic contacts[e]	CCP1: 0	CCP1: 5	CCP1: 9	CCP15: 7	CCP2: 3
	CCP2: 0	CCP2: 13	CCP2: 13	CCP16: 18	CCP3: 5
	CCP3: 13	CCP3: 10	CCP3: 20	CCP17: 23	CCP4: 26
	CCP4: 23	CCP4: 11	CCP4: 20		
	Total: 36	Total: 39	Total: 62	Total: 48	Total: 34

[a]Values reported are obtained from computational analyses using the PISA software (Krissinel & Henrick, 2007).
[b]For the C3b-CR1 (CCP15–17) and C3b-DAF (CCP2–4) structures, the values reported refer to averages between the two copies in the asymmetric unit.
[c]Values for buried surface area are defined as sum of areas from C3b and regulator.
[d]Electrostatic contacts defined as sum of residues involved in hydrogen bonds and salt bridges.
[e]Number of strong hydrophobic contacts defined as the sum of residues showing buried area percentages higher than 40% according to PISA interface analysis.

Interactions between C3b and CCP domains: sites i–ii

The N-terminal CCP domains interact with C3b only through residues from their C-terminal "bottom" and linker to the next, second CCP domain (generic CCP domains and their binding sites are referred to as CCPi-CCPiv, see Fig 2A). This CCPi–ii site constitutes a contiguous surface that interacts with a small hydrophobic patch surrounded by negatively charged residues from the α'NT region and MG7 domain on C3b (Fig EV4). The domains binding to this α'NT-MG7 site (SPICE CCP1, FH CCP1, CR1 CCP15, and DAF CCP2) differ by rigid-body rotations of 2–12° in the various complexes (Appendix Fig S4C). The diversity in domain positions yields large variations among the specific contacts observed in the C3b-regulator structures (as summarized in Fig EV2). DAF almost completely lacks hydrophobic interactions at this site, and the differences between the two C3b-DAF copies observed in crystal structure indicate weak binding of the regulator to this site (Appendix Fig S2). Previous mutagenesis data (Appendix Table S1) identified a group of amino-acid residues in DAF (located at its CCP2–CCP3 linker) as critical for decay-acceleration activity (Kuttner-Kondo *et al*, 2001). Among these, a group of positively charged residues R134-R135-K160 interacts with the α'NT of C3b in one of the two copies observed in the C3b-DAF (CCP2–4) crystal structure. In the other copy, the displacement of DAF CCP2 does not allow any contacts of this domain with C3b (Appendix Fig S2). In agreement with our data and interpretation, DAF CCP2 is not required for binding DAF to C3b (Harris *et al*, 2007), replacement of VCP CCP1 with DAF CCP2 resulted in loss of C3b binding for VCP (Ahmad *et al*, 2010), and the DAF CCP2–3 domain orientation is flexible, as shown by NMR (Uhrinova *et al*, 2003; Appendix Fig S3E). In contrast, rigidity in the domain–domain arrangement was indicated based on NMR structures of CR1 CCP15–16 and CCP16–17 (Smith *et al*, 2002), structures of related C3b-binding domains CR1 CCP1–2 and CCP2–3 (Park *et al*, 2014), and solution studies of CR1 (Furtado *et al*, 2008; Appendix Fig S3D). CR1 CCP15 shows limited but very specific interactions at this site, which are mostly localized around the loop proximate to the α'NT and the C-terminus of the CCP15 domain. These contacts constitute the specific anchoring point for CR1 CCP15–16 to the C3b platform and are consistent with previous reports (Lambris *et al*, 1996; Oran & Isenman, 1999). CR1 contacts with C3b at this site include the hydrophobic interactions surrounding CCP15 Tyr978 with α'NT Ile756 and MG7 Phe920, as well as the hydrogen bond between CCP15 Arg 980 and α'NT Asp754 (although observed only in one of the two independent complexes in the crystal). The multiple contacts observed for C3b-FH and C3b-SPICE involve few conserved and several non-conserved interactions at this site, among which electrostatic interactions and hydrophobic contacts located between the CCP1–2 interface and α'NT as well as CCP2 and MG6. These contacts include the conserved charged interaction between FH Arg83 (Arg84 in SPICE) with α'NT Glu759, the

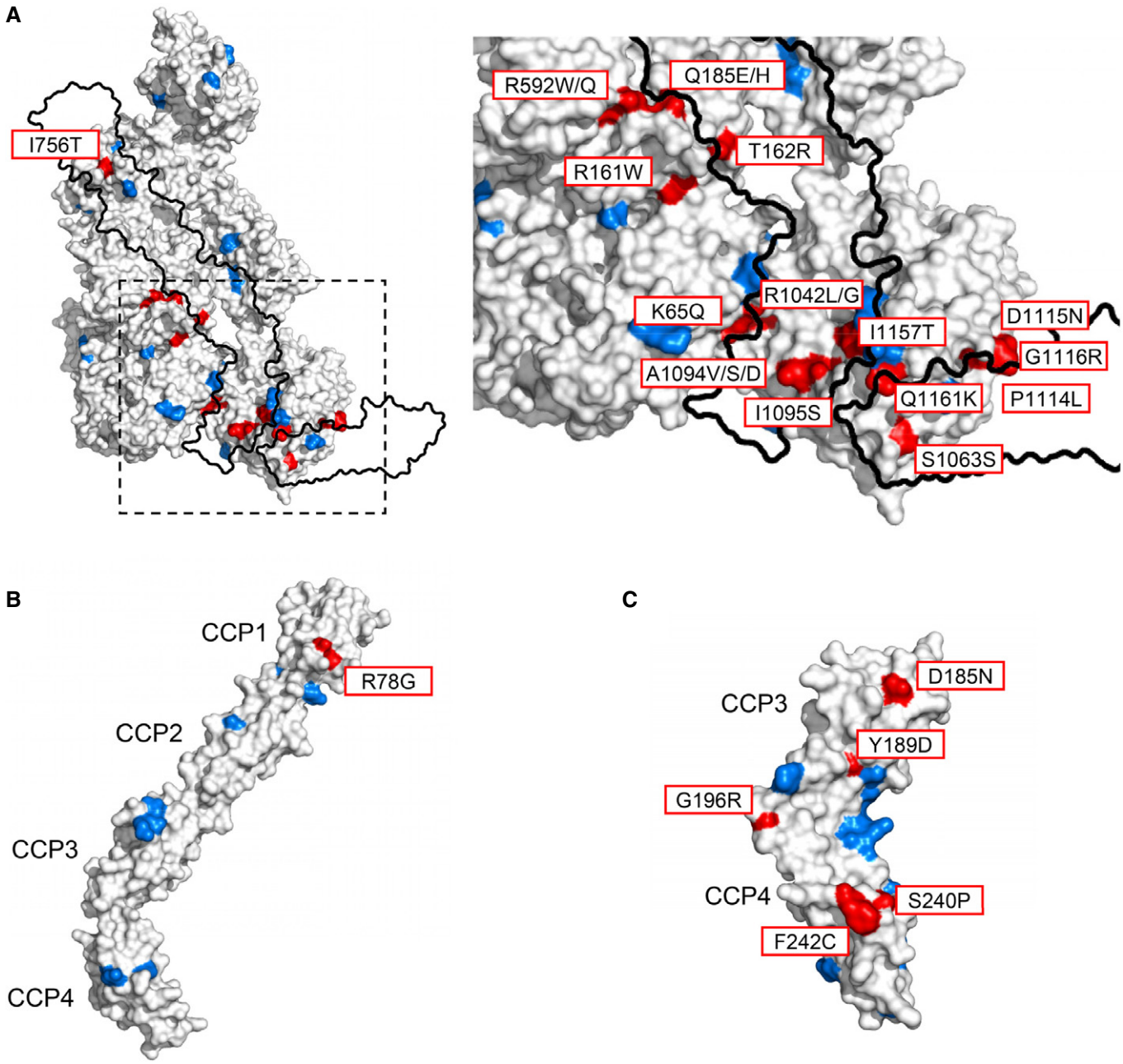

Figure 4. Structural mapping of disease-related mutations on the C3b-regulator surfaces.

A Mapping of known disease-related mutations on C3b (Appendix Table S4). The high-resolution C3b three-dimensional structure is used as structural template, shown as white surface. The regulator contact surfaces (based on C3b-FH (CCP1–4; Wu *et al*, 2009) and C3d-FH (CCP19–20; Kajander *et al*, 2011; Morgan *et al*, 2011)) are shown as black contour. All mutations reported in Appendix Table S4 are shown in blue on the C3b surface. Disease-related mutants reported to affect regulator binding are shown in red and labeled in the right magnified panel.

B Mapping of disease-related mutations on the FH (CCP1–4) surface using data from Appendix Table S5. Colors as in (A).

C Mapping of disease-related mutations on the MCP (CCP3–4) surface using data from Appendix Table S5. Colors as in (A).

hydrophobic region defined by FH Pro84-Gly86 (Arg85-Pro87 in SPICE) proximate to Val762, the conserved CCP2 residue Asp90 (Asp91 in SPICE) forming a hydrogen bond with MG6 Lys796, and the hydrophobic groove defined by FH Phe96, Leu98, and Phe104 (Leu97, Ile99, and Val102 in SPICE, respectively) with MG6 Phe794 (Fig EV2).

Interactions between C3b and CCP domains: sites ii and iii

Next, the regulator domains superposing on to FH CCP2 and CCP3 interact with domains MG2, MG6, and CUB of C3b (Fig EV2). These interactions involve polar and charged amino-acid side chains and main chain carbonyl and amino moieties of C3b MG2 forming

hydrogen bonds with the regulator domains. In particular, the β-strand formed by residues 175–186 of MG2 exposes several negative charges that form an elongated binding site, which is involved in interactions as observed in all C3b-regulator structures (Fig EV2). A fully conserved interaction is observed for main chain NH of residue Ser181 in C3b with the main chain CO of the regulator's residue preceding a sharp turn, that is, Gly171 in FH, Gly169 in SPICE, Leu184 in MCP, Gly1088 in CR1, and Arg246 in DAF. On the regulator side facing the CUB domain, amino-acid residues interacting with CUB surround residue Arg1310 of C3b, whose side chain points toward negatively charged residues (Glu177 in MCP, Glu163 in FH, Glu1083 in CR1) or aromatic side chains (Tyr162 in SPICE). In addition, highly variable interaction sub-sites are observed and are summarized in Fig EV2. Few disease-related mutations of C3 have been reported that map on the regulator binding sites formed by MG2 and MG6. The known mutations, R592W/Q, R161W, and T162R, are located on the periphery of the CCPii–iii binding regions in C3b. This CCPii–iii binding site is, however, also involved in interactions with FB at two steps in the convertase formation (Janssen *et al*, 2009; Rooijakkers *et al*, 2009; Forneris *et al*, 2010, 2012). First, in the "loading" state, FB binds C3b with its CCP2 in a position that overlaps with FH CCP2 (Janssen *et al*, 2009; Rooijakkers *et al*, 2009). Second, in the "activation" state of C3bB, the helical extension of the FB-serine protease domain covers the FH CCP3 binding site (Fig EV5; Forneris *et al*, 2010). Mutations in the CCPii–iii binding regions may thus affect both FB and FH binding to C3b. Disturbing FB binding would likely reduce or stop complement activation and, if binding of FB to C3b is still intact, disturbing FH binding would lead to uncontrolled, that is, more, complement activation. Possibly, the central role of FB binding to C3b in complement activation limits the number of disease-related mutations observed in the overlapping FB and regulator binding sites (CCPii-CCPiii) on MG2/6 of C3b.

Mutagenesis experiments on CR1 CCP clusters provided details for the putative C3b/C4b binding sites and for the residues implicated in decay-accelerating and cofactor activities (Krych *et al*, 1991, 1994, 1998; Krych-Goldberg *et al*, 1999, 2005). A summary of this comprehensive analysis is provided in Appendix Table S2 and Appendix Fig S7A–C. Consistent with our structural data, all mutations significantly affecting C3b binding in CCP8–10 and CCP15–17 map onto the C3b-CR1 (CCP15–17) interface observed in the crystal structure and are localized at C3b binding sites. Also the mutations affecting C3b/C4b binding on the CCP1–3 domains of CR1 (Appendix Table S2A) entirely map to this region. The most prominent differences between the CCP1–3 and CCP8–10, and CCP15–17 clusters are all located at the C3b-CR1 (CCP15–17) interface (Appendix Fig S7A–C). Furthermore, the epitope for the 3D9 antibody, responsible for abolishing the CR1-C3b binding (Krych *et al*, 1998), overlaps with the contact site between C3b and CR1 at the bottom side of CCP17 (Appendix Fig S7B). In DAF, mutagenesis data (summarized in Appendix Table S2 and Appendix Fig S8A) show that mutations affecting decay-acceleration activity are distributed all over the C3b-binding side of DAF, mostly through charged residues in CCP3–4 (residues R240 and R246). Domain swapping of CCP2 in the orthopox regulator Kaposica with DAF CCP3 results in loss of cofactor activity of this viral inhibitor (Gautam *et al*, 2015). The DAF side not involved in interactions with C3b shows that residues critical for decay acceleration are clustered on the CCP2–3 domains only, consistent with the expected binding data for the Bb fragment (Harris *et al*, 2007) and data from domain swapping with MCP (Gautam *et al*, 2015). Mutagenesis of SPICE and the homologous VCP (Yadav *et al*, 2008; Liszewski *et al*, 2009; Appendix Table S3) indicated that SPICE residue Asn163 (located on CCP3) is solely responsible for a four-fold increase in C3b binding, when replaced with Glu163 in VCP (Sfyroera *et al*, 2005; Yadav *et al*, 2008). In the C3b-SPICE (CCP1–4) structure, this residue lies at the interface between C3b and SPICE, in the vicinity of MG2 Asp178 side chain (although not forming hydrogen bonds with this residue; Fig 3E). Hence, the presence of a negatively charged residue in VCP in this position may be responsible for the reduced binding affinity due to charge repulsion, as initially suggested by previous computational electrostatic modeling of VCP and SPICE chimeras (Sfyroera *et al*, 2005).

Interactions between C3b and CCP domains: site iv

A C-terminal interaction site is observed for FH, MCP, and SPICE CCP4 with MG1 and TED domains of C3b. As described above, the most prominent feature of this interaction site is the marked structural difference in the orientation of the CCP4 domains of MCP and SPICE binding to C3b compared to FH. Moreover, the high B-factors for C3b-SPICE at this interaction site suggest flexibility and reduced interactions between SPICE CCP4 and C3b in comparison with the FH and MCP. SPICE CCP4 bears numerous negative charges at the bottom-edge of this domain in comparison with FH and MCP (Fig EV4). Remarkably, removal of one of the few positive charges located in the observed contact interface with C3b at the "bottom" of VCP CCP4 (residue Lys233, corresponding to SPICE Thr233, Fig 3E) did not affect C3b binding (Yadav *et al*, 2008). This observation supports the notion that SPICE CCP4 contributes less to complex formation. SPICE and the highly homologous VCP are evolutionarily more closely related to MCP than to other human regulators (Ciulla *et al*, 2005). This is in agreement with the structural arrangement observed in C3b-SPICE (CCP1–4), which shows strong similarity to MCP in the orientation of the CCP3 and CCP4 domains bound to C3b (Fig 3A and B). Whereas charged residues are broadly distributed over the whole interaction surface of FH CCP4 providing interactions with both MG1 and TED, MCP and SPICE are binding to C3b only through the upper half of their CCP4 domains and only with TED, that is, without specific interactions with the MG1 domain of C3b (Fig EV2B).

Mapping disease-related mutations and disease-predisposing polymorphisms

Over the years, a large number of mutations and disease-predisposing polymorphisms associated with pathological conditions such as aHUS, AMD, and C3G have been reported involving C3b and/or complement regulators FH and MCP (summarized in Appendix Tables S4 and S5). Our structures enable precise mapping and provide a structural interpretation of the effects for the majority of these mutations. Except for those clearly identified as involved in binding of FH CCP19–20 (Jokiranta *et al*, 2000; Kajander *et al*, 2011; Morgan *et al*, 2011), all pathogenic C3b mutations known to affect regulator-C3b binding map on residues

located on MG1, MG2, MG6, and MG7 at or near the regulator binding interface (Fig 4A). Our data now facilitate a structural basis to observed functional differences between regulators due to these mutations. C3G-related deletion mutation 923-ΔDG located on MG7 of C3b (Martinez-Barricarte *et al*, 2010) influences the conformation of the α'NT region. This region provides critical contact sites for FH, whereas the structural variability observed in the two C3b-DAF (CCP2–4) monomers found in the crystal structure of the complex indicates that this region is dispensable for DAF binding (Appendix Fig S8B). Consistently, this mutation impairs decay acceleration and binding by FH, but not by DAF (Martinez-Barricarte *et al*, 2010). aHUS mutations Q185E/H on MG2 (Noris *et al*, 2010) and R592Q on MG6 (Fremeaux-Bacchi *et al*, 2008; Fig 4A) affect binding and cofactor activity of FH, but not those of MCP nor CR1 (Schramm *et al*, 2015; Appendix Table S4). In C3b-FH, these C3b mutations disrupt the hydrogen bonds with the side chain of residue Glu116 on CCP2 (Wu *et al*, 2009). Such hydrogen-bonding network is not present in C3b-MCP or C3b-CR1, as shown by the very weak and flexible interactions of MCP CCP2, and the presence of a threonine residue (CCP16 residue 1,033) in CR1 replacing FH Glu116 (Fig EV2B). Mutations on regulators can be divided into two major groups in general. One group maps onto the C3b-regulator interfaces and likely affects interactions with C3b, whereas the second group is located on the opposite side of the regulator and cannot be explained by current structural data. The latter mutations likely affect the interactions of the regulator with factor I in cofactor activity or with the convertase fragment Bb in decay-acceleration activity. Despite extensive studies on pathogenic mutations of FH located on its CCP1–4 domains (summarized in Appendix Table S5), their effects on C3b binding were only studied for very few mutations. The V62I mutation showed increased binding affinity for C3b and enhanced cofactor activity (Tortajada *et al*, 2009). Pechtl *et al* (2011) found that aHUS mutation R78G has the opposite effect, reducing FH binding to C3b, as well as cofactor and decay-accelerating activity. As we already reported for the C3b-FH (CCP1–4) crystal structure (Wu *et al*, 2009), this mutation maps in the middle of the C3b-FH contact interface at the CCP1 site (Fig 4B). In MCP, numerous pathogenic mutations leading to aHUS and C3G phenotypes affect domains CCP3 and CCP4 (Appendix Table S5). For five of these mutations, all associated with aHUS, binding studies report reduced C3b binding and decreased cofactor activity (Richards *et al*, 2003; Caprioli *et al*, 2006; Fremeaux-Bacchi *et al*, 2006). Consistent with our structural data, these five mutations are located at the C3b-MCP contact sites, as shown in Fig 4C. In CR1, the only documented mutation in the CCP15–17 region is Q1022H, which may be linked to adaptive evolutionary events to protect individuals from cerebral malaria in endemic regions of Asia (Birmingham *et al*, 2003; Thomas *et al*, 2005). This mutation is located on CCP16, in proximity to the CCP15–16 linker, and is conserved in all three CR1 CCP clusters that bind C3b (Appendix Fig S7A). Presence of this mutation increases CR1 binding affinity to C4b but not to C3b (Birmingham *et al*, 2003). In the C3b-CR1 (CCP15–17) structure, this residue is in close proximity (approximately 6 Å) to C3b, but does not make direct contacts with C3b (Appendix Fig S7D). Superposition with the recently published three-dimensional structure of C4b (Mortensen *et al*, 2015), however, does not suggest a straightforward explanation for the alteration in CR1-C4b binding affinity due to this mutation.

Conclusions

The four presented and one previously published crystal structures of C3b-regulator complexes show that the consecutive CCP domains harboring the complement-inhibitory activities of human MCP, DAF, FH, CR1, and of vaccinia virus-derived SPICE bind in the same orientation to the same binding platform on C3b. Nevertheless, marked deviations from the common binding mode are apparent with differences in participation of individual domains to the binding (consistent with biochemical data) and in virtually all details of the interacting residues at the C3b-regulator interface.

The largest known binding platform on C3b for regulator fragments stretches from the α'NT-MG7 site, through sites on MG6, MG2, and CUB to MG1 and TED, as previously observed for C3b-FH (CCP1–4; Wu *et al*, 2009), with an additional binding site for FH (CCP19–20) at TED (Jokiranta *et al*, 2000; Kajander *et al*, 2011; Morgan *et al*, 2011). The CCP1–CCP4 domains of FH and SPICE bind with the N-terminal domains (CCP1) to the α'NT-MG7 site, CCP2 to MG6-MG7, CCP3 to MG2 and CUB, and the C-terminal CCP4 to MG1 and TED, defining the generic CCPi-CCPiv domains and binding sites. MCP only binds through its CCP3–4 domains at the CCPiii-CCPiv binding sites on C3b. The orientation of MCP and SPICE CCP4 differs by 100° from that of FH however without changing the overall global binding of the extended CCP configuration and, thus, adhering to the common binding mode. The domains CCP2–4 of DAF and CCP15–17 of CR1 bind at the sites CCPi–iii, in agreement with biochemical binding data (Krych *et al*, 1994; Harris *et al*, 2007; Gautam *et al*, 2015). The similarity in C3b binding of the decay-accelerating regulator DAF, cofactor–regulator MCP and CR1 (CCP15–17), and dual-activity regulators FH and SPICE suggests that the two distinct complement-inhibition mechanisms (decay-acceleration and cofactor activities) may have evolved from a common C3b-regulator binding origin. Furthermore, the strong decay accelerator DAF binds both C3b and Bb and both binding sites appear important for decay activity (Harris *et al*, 2007). However, what the roles of the two binding sites are in the molecular mechanism of decay acceleration remains unclear. Based on sequence and structural homologies, the regulators of the classical pathway of complement activation (that is thought to have evolved from the alternative pathway (Nonaka & Yoshizaki, 2004)) likely bind C4b using the same binding mode as in C3b-regulator binding. The extensive variations during evolution may have served to adapt precise regulator functionality. Concatenation of the three C3b/C4b binding sites in CR1 may provide synergistic effects (Krych-Goldberg *et al*, 2005). The fluid regulator FH may have adapted its CCP4 orientation from a putative canonical orientation as observed for MCP CCP4 and SPICE CCP4, to account for subsequent CCP domains involved in host interactions of the soluble FH. Similarly, the surface-bound regulators MCP and DAF may have evolved to enhance their cofactor- and decay-acceleration activity, respectively, at the expense of losing the potential of dual function. Thus, we conclude that the two functional activities, decay-acceleration and cofactor activities, are based on one common C3b-regulator binding mode.

Regulators with decay-acceleration and/or cofactor activity vary in CCP domains bound to the CCPi–iv binding sites on C3b. Biochemical data (Krych *et al*, 1991, 1994; Gordon *et al*, 1995; Kuttner-Kondo *et al*, 2001, 2007; Harris *et al*, 2007; Wu *et al*, 2009; Gautam *et al*, 2015) show that domains CCPi-CCPiii suffice for decay-accelerating activity. The structural data support the observation that predominantly CCPii–iii (as for DAF CCP3–4) account for the C3b binding interactions (Harris *et al*, 2007). Domains CCPi-ii (CCP2–3) of DAF are important for binding the Bb protease fragment (Kuttner-Kondo *et al*, 2003; Harris *et al*, 2007); thus, CCPi–iii form a minimal functional fragment in decay acceleration (Kuttner-Kondo *et al*, 2001, 2007; Harris *et al*, 2007). Strong cofactor activity of MCP requires binding of only CCP3–4 to sites CCPiii–iv (Liszewski *et al*, 2000; Gautam *et al*, 2015). Nevertheless, an associated CCPii domain is linked to cofactor activity (Krych *et al*, 1994, 1998; Yadav *et al*, 2008; Gautam *et al*, 2015); presumably, it is required for binding of FI. Regulators with both decay acceleration and cofactor activity bind C3b through CCPi up to CCPiv: This combines C3b binding interaction at CCPi–ii for decay acceleration and those for cofactor activity at CCPiii–iv for regulator activity.

Structures of C3b with MCP, FH, or SPICE reveal many interactions with C3b at the CCPiii binding site. At the CCPiv site, the CCP4 domains of FH, MCP, and SPICE differ in interactions with C3b. MCP and SPICE CCP4 bind in the same orientation and interact with TED. FH CCP4 differs by ~100° (around the longitudinal axis) and interacts with both MG1 and TED. The density and B-factor for CCP4 of SPICE suggest weaker binding for SPICE at this site. In the structures of C3b-FH (CCP1–4) and C3b-MCP, the interactions of CCP4 with TED appear correlated with a 6–9 Å tilt of CUB-TED. In addition, this lifting of CUB-TED facilitates interactions between MG2, CUB, and CTC. The CUB-CTC arrangement in the latter two C3b complexes is remarkably similar to the CUB-CTC contact in native C3. Moreover, interactions bridging MG2-CUB induced by regulators with cofactor activity may be critical for FI binding and cofactor activity (Gautam *et al*, 2015). However, whether and how these conformational changes affect the cofactor activity requires structural data of the ternary complex of C3b-regulator with a bound FI.

Our data are in good agreement with mutagenesis and functional characterizations of regulator-C3b binding (Krych *et al*, 1991, 1994, 1998; Krych-Goldberg *et al*, 1999, 2005; Liszewski *et al*, 2000; Kuttner-Kondo *et al*, 2001, 2007; Sfyroera *et al*, 2005; Harris *et al*, 2007; Yadav *et al*, 2008; Ahmad *et al*, 2010; Gautam *et al*, 2015). Moreover, the presented structural data explain the differential effect of C3b mutations on regulators. Depending on the location of the mutant in the extended binding site, some but not all regulators may be affected by that mutation (Martinez-Barricarte *et al*, 2010; Schramm *et al*, 2015). Disease-related mutations affecting C3b-regulator interactions are located at or near the CCP interaction sites. Most mutations are located near the CCPiv site, while CCPii and CCPiii have less disease-related mutations known to date. The CCPii and CCPiii sites, however, also provide a contact interface for FB in convertase formation, both in the "loading" and "activated" conformation of FB bound to C3b (Fig EV5). Perhaps, the C3b interactions with FB (preceding the interactions with regulators in the complement pathways) restrict the number of mutations affecting regulator binding at the CCPii and CCPiii sites. Mutations in FH, MCP, and CR1 affecting FI binding (Krych *et al*, 1991; Krych-Goldberg *et al*, 1999; Liszewski *et al*, 2000; Rodriguez *et al*, 2014) or in DAF affecting Bb binding (Kuttner-Kondo *et al*, 2003; Harris *et al*, 2007) are distant from the observed C3b-regulator interfaces; thus, the structural data support the interpretation that these mutation affect either FI or Bb interactions. We could, however, not confirm previously reported C3b interactions or regulator activity for β2GPI (Gropp *et al*, 2011; Fig EV1). Even though CCP1–4 of β2GPI resembles complement regulators in domain composition and overall shape, its amino-acid composition differs markedly from complement regulators of the RCA family. In particular, the putative C3b-binding site on CCP3 displays numerous hydrophobic residues, where regulators contain hydrophilic residues critical for C3b binding (Appendix Fig S9A). Furthermore, β2GPI Asn162 in CCP3 is glycosylated (Bouma *et al*, 1999), whereas residues at the equivalent site of the regulators are interacting with C3b (Appendix Fig S9B). Thus, the Asn162 linked glycan of β2GPI likely precludes binding to C3b.

In summary, we have shown that C3b-regulator binding can be classified as extensive variations on a common binding mode. We hypothesize that one evolutionary origin may underlie this C3b-regulator binding mode that facilitates both decay-acceleration and cofactor activities in complement inhibition for host protection or immune evasion. The data highlight how molecular mimicry may impact infection and immunity, that is, how the evolution of structural and functional similarities of SPICE from variola virus, and homologs from other orthopox viruses, with human RCA assists its evasion of complement response (Ahmad *et al*, 2007; Ojha *et al*, 2014). Finally, the presented structural data will be instrumental to characterize the functional consequences of genetic polymorphisms (Rodriguez *et al*, 2014) that have been associated with pathologies and may guide the further development of regulator-based therapeutics for the treatment of complement-mediated diseases (Ricklin & Lambris, 2013b).

Materials and Methods

Protein production and C3b affinity measurements

Complement component C3b was obtained by isolating C3 from fresh human plasma, followed by specific cleavage of C3 into C3b by recombinant human factor B and factor D as described before (Forneris *et al*, 2010). Iodoacetamide was used to block the nascent thioester to prevent dimerization of C3b. The regulator fragments were produced in *E. coli*, *P. pastoris,* and human embryonic kidney (HEK) 293 cells. CR1 CCP15–17 (residues 942–1,136) was produced in *P. pastoris* using established methods (Kirkitadze *et al*, 1999). MCP CCP1–4 (residues 35–285), and full-length SPICE CCP1–4 (residues 19–263) were expressed in inclusion bodies in *E. coli*, refolded and purified (Sfyroera *et al*, 2005; Fremeaux-Bacchi *et al*, 2008). N-terminal His_6-tagged DAF CCP2–4 (residues 97–285) and MCP CCP1–4 (residues 35–285), as glycosylated alternative to the *E. coli* product, were purified from medium after expression in HEK293. Purified MCP (CCP1–4) from both *E. coli* and HEK293 showed comparable activity (Fig EV1), confirming previous observations that glycosylation at the three potential glycosylation sites does not affect cofactor activity (Liszewski *et al*, 1998). Full-length β2-glycoprotein I (β2GPI) and its fragment CCP1–4 were recombinantly

expressed in HEK293 cells. For crystallization purposes, we used N-acetylglucosaminyltransferase I-negative HEK293 cells (HEK293-ES, U-Protein Express B.V. Utrecht, the Netherlands; Reeves *et al*, 2002), which lack the ability to synthesize complex Asn-linked glycans and hence produce short-chain, and more homogeneous, glycosylated proteins that can be crystallized more readily. All proteins were purified to homogeneity by either metal-affinity chromatography or ion-exchange chromatography and gel-filtration prior to crystallization according to previously established protocols (Wu *et al*, 2009; Forneris *et al*, 2010).

C3b binding affinity of the purified regulator proteins and protein fragments was determined by surface plasmon resonance (SPR), using a Biacore 3000 instrument (GE Healthcare) at 25°C. As described previously (Schmidt *et al*, 2013), C3b was deposited through its thioester moiety onto CM5 sensor chips by covalently immobilizing a low amount of C3b (< 500 RU) on a flow cell using standard amine coupling chemistry and amplifying C3b deposition via multiple injection cycles of factors B and D (200 nM each) and C3 (1 μM) in HBST buffer (10 mM HEPES, 150 mM NaCl, 0.005% Tween-20, pH 7.4) containing 1 mM $NiCl_2$. Comparative affinity measurements of complement regulators were performed in HBST containing 3 mM EDTA as running buffer. Twofold serial dilutions of MCP CCP1–4 (0.003–7 μM), both from *E. coli* and HEK293, FH CCP1–4 (0.005–19 μM), CR1 CCP15–17 (0.005–11 μM), DAF CCP1–4 (0.09–50 μM), and SPICE CCP1–4 (0.003–3.5 μM) were injected for 60 s at a flow rate of 20 μl/min with a dissociation phase of 180 s. No regeneration was required as all signals readily returned to baseline. Data were processed and analyzed in Scrubber (v2.0c; BioLogic Software). An unmodified CM5 sensor chip flow cell was used as a reference surface, and several buffer blank injections were subtracted to account for buffer bulk and injection artifacts. Injection signals were normalized by dividing the SPR responses by the molecular weight of the corresponding protein. Binding affinities (K_D) were calculated by globally fitting the processed steady state responses of the regulators to a single-site binding model. In the case of β2GPI, the binding activity toward C3b and the proposed property to enhance the interaction between C3b and FH were assessed on a CM5 sensor chip surface with covalently immobilized C3b. For this purpose, β2GPI CCP1–4 was injected at a concentration of 500 nM for 2 min at a flow rate of 10 μl/min with a dissociation phase of 2 min. Three concentrations of FH (12.5, 25, 50 nM) were injected under the same conditions in the presence and absence of 500 nM β2GPI CCP1–4. The surface was regenerated by injecting 2 M NaCl for 60 s after each cycle. The data were analyzed using Scrubber as described above.

Protein crystallization and structure determination

Crystallizations of the C3b-regulators were performed by vapor diffusion at 18°C in 1:1 molar ratios to protein concentrations of 8–10 mg/ml. Crystals of C3b and *E. coli*-derived MCP (CCP1–4) were obtained in droplets equilibrated against 100 mM ammonium citrate, 7% w/v polyethylene glycol (PEG) 3350, 5 mM L-glutathione, and 50 mM bis-Tris propane, pH 6.5. Crystals appeared after 2–3 days and were harvested from mother liquor solution after 1 week. Initial crystals for C3b-SPICE were obtained at 75 mM ammonium iodide and 3.5% w/v PEG 3350, but these crystals diffracted poorly. Well-diffracting crystals were obtained after seeding the initial crystal hits in fresh crystallization droplets. The crystals appeared after few hours and continued to grow for about 1 week. First attempts to crystallize C3b-CR1 (CCP15–17) yielded good quality crystals containing free C3b. Further experiments yielded crystals of C3b-CR1 (CCP15–17) using a reservoir composed of 8% w/v PEG 3350 and 35 mM bis-Tris pH 5.5. For C3b-DAF (CCP2–4), crystals suitable for diffraction were obtained after extensive microseed-matrix screening (Till *et al*, 2013) in a condition containing 60 mM $MgCl_2$, 30 mM bis-Tris pH 5.5, 6.5% w/v PEG 3350, and 3% v/v meso-erythritol, using sitting drop vapor diffusion at 30°C.

All crystals were harvested using nylon cryo-loops, transferred to reservoir solutions supplemented with cryo-protectants (20% v/v ethylene glycol for C3b-MCP (CCP1–4), 20–25% w/v glycerol for C3b-SPICE (CCP1–4), C3b-CR1 (CCP15–17), and C3b-DAF (CCP2–4) and flash-frozen in liquid nitrogen for data collection. Diffraction data were collected at beamlines of the European Synchrotron Radiation Facility (ESRF) and the Swiss Light Source (SLS; details in Table 1) and processed using MOSFLM, XDS, and AIMLESS (Collaborative Computational Project, Number 4, 1994; Kabsch, 2010; Battye *et al*, 2011). The observed resolution limits of the diffraction data, selected by evaluating the correlations between half data sets (CC1/2; Karplus & Diederichs, 2012), were 2.8 Å for C3b, 2.4 Å for C3b-MCP (CCP1–4), 2.5 Å for C3b-SPICE (CCP1–4), 3.3 Å for C3b-CR1 (CCP15–17), and 4.2 Å for C3b-DAF (CCP2–4). All structures were solved by molecular replacement by Phaser (McCoy *et al*, 2007) using the coordinates from the crystal structures C3c minus its CTC domain (PDB ID 2A74; Janssen *et al*, 2005), followed by sequential positioning of the TED, CTC, and CUB domains obtained from the three-dimensional structure of C3b (PDB ID 2I07; Janssen *et al*, 2006). Search models for regulators were generated from the crystal structures of MCP (CCP1–4; PDB ID 3O8E; Persson *et al*, 2010), DAF (CCP1–4; PDB ID 1OK3; Lukacik *et al*, 2004), and the NMR structures of CR1 (CCP15–16 and CCP16–17; PDB IDs 1GKN and 1GKG, resp.; Smith *et al*, 2002). Alternating cycles of automated refinement using phenix.refine (Adams *et al*, 2010) and manual model building using COOT (Emsley *et al*, 2010) were applied to generate the structural models. Validation of the final structural models was carried out using MOLPROBITY (Chen *et al*, 2010) and PDB-CARE (Lutteke & von der Lieth, 2004). Complete data collection details and final model statistics are available in Table 1. In all structures, all domains of C3b could be modeled (Appendix Fig S2). For C3b-MCP (CCP1–4), only domains CCP3–4 of MCP could be modeled due to lack of density for CCP1 and lack of interpretable density for CCP2 (Fig 1D). All four CCP domains of SPICE were modeled; however, CCP4 showed notably weak density (Fig 1D). Two C3b-CR1 (CCP15–17) complexes were present in the asymmetric unit. The two C3b-CR1 (CCP15–17) complexes displayed minor differences in the orientation of domain CCP15, while neither of the two copies of CCP15 was directly involved in crystal contacts. Non-crystallographic symmetry was applied to each CCP domain of CR1 separately (excluding the linker peptides), thus allowing adjustment of the binding orientations and positions of the CCP domains with respect to C3b in each copy. Also for C3b-DAF (CCP2–4), two copies of the complex were present in the asymmetric unit with significant differences in orientation of the CCP2 and CCP3 domains. Extensive crystal contacts between CCP2 of one copy with CCP4 of another resulted in 17° rotation of the regulator (compared to its bound C3b)

and a displacement of over 20 Å (as measured at the N-terminal edge of CCP2; Appendix Fig S2A). For modeling and refinement against the 4.2-Å resolution C3b-DAF (CCP2–4) data set, external structural restraints were applied based on the 2.8 Å-resolution C3b structure (this work) and the high-resolution structures of free DAF (Lukacik *et al*, 2004).

Coordinates and structure factors for C3b and the complexes of C3b-MCP (CCP1–4), C3b-CR1 (CCP15–17), C3b-DAF (CCP2–4), and C3b-SPICE (CCP1–4) have been deposited at the Protein Data Bank (PDB) with accession numbers 5FO7, 5FO8, 5FO9, 5FOA, and 5FOB, respectively. For consistency, UniProt residue numberings were used throughout, including in the deposited structure coordinates. We refer to the sequences of UniProt database entries P01024 (C3/C3b), P15529 (MCP), Q89859 (SPICE), P08603 (FH), P17927 (CR1), P08174 (DAF), and P02749 (β2GPI). The reference sequence for the vaccinia virus complement control protein (VCP) used for comparison with SPICE was UniProt entry P68638.

Expanded View for this article is available online.

Acknowledgements

We gratefully thank the European Synchrotron Radiation Facility (ESRF) and the Swiss Light Source (SLS) for the provision of synchrotron radiation facilities and beamline scientists of the ESRF, SLS, and the European Molecular Biology Laboratory for assistance. We thank Malgorzata Krych for assistance in the production and purification of CR1 (CCP15–17). We thank Elizabeth Schramm for reviewing C3 mutations. This work was supported by a "Top" grant (700.54.304 to P.G.) by the Council for Chemical Sciences of the Netherlands Organization for Scientific Research (NWO-CW), the European Research Council (grant no. 233229), the European Community's Seventh Framework Programmes (FP7/2007–2013) under BioStruct-X (grant no. 283570) and FP7/DIREKT (grant no. 602699; to J.D.L.), and grants by the National Institutes of Health (AI068730, AI030040; to J.D.L.) and the National Science Foundation (no. 1423304; to D.R.). Grant support was also provided for J.P.A. by the National Institutes of Health (R01 grant GM0099111), National Heart, Lung, and Blood Institute, part of the National Institutes of Health (U54 grant GK112303-03) and by the National Institute of Arthritis and Musculoskeletal and Skin Diseases, part of the National Institutes of Health, under Award Number P30AR048335 for the Protein Production Facility of the Rheumatic Diseases Core Center at Washington University in Saint Louis. Note: "The content is solely the responsibility of the authors and does not necessarily represent the official views of the National Institutes of Health". E.V. was supported by the Dutch Kidney Foundation (13OI116, KFB 11.007, IP 10.22) and ERA-EDTA (ERA LTF 203-2014).

Author contributions

JW, FF, and XX purified C3b. XX and JCMG purified DAF(2–4). RH, PB, and MKL produced and purified CR1. GS produced and purified MCP and SPICE. FF produced and purified β2GPI. JW crystallized and solved the structures of C3b-CR1, C3b-MCP, and C3b-SPICE. XX crystallized and solved the structure of C3b-DAF. FF refined and analyzed all structural data. DR, ZL, and AT performed surface plasmon resonance experiments and analysis. EV and JPA assisted in interpretation of genetic data. FF prepared figures. JDL and PG supervised the project. FF, DR, XX, and PG performed data analysis and interpretation and wrote the manuscript.

Conflict of interest

The authors declare that they have no conflict of interest.

References

Adams EM, Brown MC, Nunge M, Krych M, Atkinson JP (1991) Contribution of the repeating domains of membrane cofactor protein (CD46) of the complement system to ligand binding and cofactor activity. *J Immunol* 147: 3005 – 3011

Adams PD, Afonine PV, Bunkoczi G, Chen VB, Davis IW, Echols N, Headd JJ, Hung LW, Kapral GJ, Grosse-Kunstleve RW, McCoy AJ, Moriarty NW, Oeffner R, Read RJ, Richardson DC, Richardson JS, Terwilliger TC, Zwart PH (2010) PHENIX: a comprehensive Python-based system for macromolecular structure solution. *Acta Crystallogr D Biol Crystallogr* 66: 213 – 221

Ahmad M, Pyaram K, Mullick J, Sahu A (2007) Viral complement regulators: the expert mimicking swindlers. *Indian J Biochem Biophys* 44: 331 – 343

Ahmad M, Raut S, Pyaram K, Kamble A, Mullick J, Sahu A (2010) Domain swapping reveals complement control protein modules critical for imparting cofactor and decay-accelerating activities in vaccinia virus complement control protein. *J Immunol* 185: 6128 – 6137

Aleshin AE, DiScipio RG, Stec B, Liddington RC (2012) Crystal structure of C5b-6 suggests structural basis for priming assembly of the membrane attack complex. *J Biol Chem* 287: 19642 – 19652

Baker NA, Sept D, Joseph S, Holst MJ, McCammon JA (2001) Electrostatics of nanosystems: application to microtubules and the ribosome. *Proc Natl Acad Sci USA* 98: 10037 – 10041

Battye TG, Kontogiannis L, Johnson O, Powell HR, Leslie AG (2011) iMOSFLM: a new graphical interface for diffraction-image processing with MOSFLM. *Acta Crystallogr D Biol Crystallogr* 67: 271 – 281

Birmingham DJ, Chen W, Liang G, Schmitt HC, Gavit K, Nagaraja HN (2003) A CR1 polymorphism associated with constitutive erythrocyte CR1 levels affects binding to C4b but not C3b. *Immunology* 108: 531 – 538

Bouma B, de Groot PG, van den Elsen JM, Ravelli RB, Schouten A, Simmelink MJ, Derksen RH, Kroon J, Gros P (1999) Adhesion mechanism of human beta(2)-glycoprotein I to phospholipids based on its crystal structure. *EMBO J* 18: 5166 – 5174

Caprioli J, Noris M, Brioschi S, Pianetti G, Castelletti F, Bettinaglio P, Mele C, Bresin E, Cassis L, Gamba S, Porrati F, Bucchioni S, Monteferrante G, Fang CJ, Liszewski MK, Kavanagh D, Atkinson JP, Remuzzi G (2006) Genetics of HUS: the impact of MCP, CFH, and IF mutations on clinical presentation, response to treatment, and outcome. *Blood* 108: 1267 – 1279

Chen VB, Arendall WB 3rd, Headd JJ, Keedy DA, Immormino RM, Kapral GJ, Murray LW, Richardson JS, Richardson DC (2010) MolProbity: all-atom structure validation for macromolecular crystallography. *Acta Crystallogr D Biol Crystallogr* 66: 12 – 21

Ciulla E, Emery A, Konz D, Krushkal J (2005) Evolutionary history of orthopoxvirus proteins similar to human complement regulators. *Gene* 355: 40 – 47

Clark SJ, Ridge LA, Herbert AP, Hakobyan S, Mulloy B, Lennon R, Wurzner R, Morgan BP, Uhrin D, Bishop PN, Day AJ (2013) Tissue-specific host recognition by complement factor H is mediated by differential activities of its glycosaminoglycan-binding regions. *J Immunol* 190: 2049 – 2057

Collaborative Computational Project, Number 4 (1994) The CCP4 suite: programs for protein crystallography. *Acta Crystallogr D Biol Crystallogr* 50: 760 – 763

Dragon-Durey MA, Blanc C, Garnier A, Hofer J, Sethi SK, Zimmerhackl LB (2010) Anti-factor H autoantibody-associated hemolytic uremic syndrome: review of literature of the autoimmune form of HUS. *Semin Thromb Hemost* 36: 633 – 640

Dragon-Durey MA, Fremeaux-Bacchi V (2005) Atypical haemolytic uraemic syndrome and mutations in complement regulator genes. *Springer Semin Immunopathol* 27: 359 – 374

Emsley P, Lohkamp B, Scott WG, Cowtan K (2010) Features and development of Coot. *Acta Crystallographica Section D* 66: 486 – 501

Forneris F, Ricklin D, Wu J, Tzekou A, Wallace RS, Lambris JD, Gros P (2010) Structures of C3b in complex with factors B and D give insight into complement convertase formation. *Science* 330: 1816 – 1820

Forneris F, Wu J, Gros P (2012) The modular serine proteases of the complement cascade. *Curr Opin Struct Biol* 22: 333 – 341

Fredslund F, Jenner L, Husted LB, Nyborg J, Andersen GR, Sottrup-Jensen L (2006) The structure of bovine complement component 3 reveals the basis for thioester function. *J Mol Biol* 361: 115 – 127

Fredslund F, Laursen NS, Roversi P, Jenner L, Oliveira CL, Pedersen JS, Nunn MA, Lea SM, Discipio R, Sottrup-Jensen L, Andersen GR (2008) Structure of and influence of a tick complement inhibitor on human complement component 5. *Nat Immunol* 9: 753 – 760

Fremeaux-Bacchi V, Miller EC, Liszewski MK, Strain L, Blouin J, Brown AL, Moghal N, Kaplan BS, Weiss RA, Lhotta K, Kapur G, Mattoo T, Nivet H, Wong W, Gie S, Hurault de Ligny B, Fischbach M, Gupta R, Hauhart R, Meunier V *et al* (2008) Mutations in complement C3 predispose to development of atypical hemolytic uremic syndrome. *Blood* 112: 4948 – 4952

Fremeaux-Bacchi V, Moulton EA, Kavanagh D, Dragon-Durey MA, Blouin J, Caudy A, Arzouk N, Cleper R, Francois M, Guest G, Pourrat J, Seligman R, Fridman WH, Loirat C, Atkinson JP (2006) Genetic and functional analyses of membrane cofactor protein (CD46) mutations in atypical hemolytic uremic syndrome. *J Am Soc Nephrol* 17: 2017 – 2025

Furtado PB, Huang CY, Ihyembe D, Hammond RA, Marsh HC, Perkins SJ (2008) The partly folded back solution structure arrangement of the 30 SCR domains in human complement receptor type 1 (CR1) permits access to its C3b and C4b ligands. *J Mol Biol* 375: 102 – 118

Garcia BL, Ramyar KX, Tzekou A, Ricklin D, McWhorter WJ, Lambris JD, Geisbrecht BV (2010) Molecular Basis for Complement Recognition and Inhibition Determined by Crystallographic Studies of the Staphylococcal Complement Inhibitor (SCIN) Bound to C3c and C3b. *J Mol Biol* 402: 17 – 29

Gautam AK, Panse Y, Ghosh P, Reza MJ, Mullick J, Sahu A (2015) Mutational analysis of Kaposica reveals that bridging of MG2 and CUB domains of target protein is crucial for the cofactor activity of RCA proteins. *Proc Natl Acad Sci USA* 112: 12794 – 12799

Gordon DL, Kaufman RM, Blackmore TK, Kwong J, Lublin DM (1995) Identification of complement regulatory domains in human factor H. *J Immunol* 155: 348 – 356

Gropp K, Weber N, Reuter M, Micklisch S, Kopka I, Hallstrom T, Skerka C (2011) beta(2)-glycoprotein I, the major target in antiphospholipid syndrome, is a special human complement regulator. *Blood* 118: 2774 – 2783

Hadders MA, Bubeck D, Roversi P, Hakobyan S, Forneris F, Morgan BP, Pangburn MK, Llorca O, Lea SM, Gros P (2012) Assembly and regulation of the membrane attack complex based on structures of C5b6 and sC5b9. *Cell Rep* 1: 200 – 207

Harris CL, Abbott RJ, Smith RA, Morgan BP, Lea SM (2005) Molecular dissection of interactions between components of the alternative pathway of complement and decay accelerating factor (CD55). *J Biol Chem* 280: 2569 – 2578

Harris CL, Pettigrew DM, Lea SM, Morgan BP (2007) Decay-accelerating factor must bind both components of the complement alternative pathway C3 convertase to mediate efficient decay. *J Immunol* 178: 352 – 359

Hebecker M, Alba-Dominguez M, Roumenina LT, Reuter S, Hyvarinen S, Dragon-Durey MA, Jokiranta TS, Sanchez-Corral P, Jozsi M (2013) An engineered construct combining complement regulatory and surface-recognition domains represents a minimal-size functional factor H. *J Immunol* 191: 912 – 921

Heurich M, Martinez-Barricarte R, Francis NJ, Roberts DL, Rodriguez de Cordoba S, Morgan BP, Harris CL (2011) Common polymorphisms in C3, factor B, and factor H collaborate to determine systemic complement activity and disease risk. *Proc Natl Acad Sci USA* 108: 8761 – 8766

Hourcade DE, Mitchell LM, Medof ME (1999) Decay acceleration of the complement alternative pathway C3 convertase. *Immunopharmacology* 42: 167 – 173

Janssen BJ, Christodoulidou A, McCarthy A, Lambris JD, Gros P (2006) Structure of C3b reveals conformational changes that underlie complement activity. *Nature* 444: 213 – 216

Janssen BJ, Gomes L, Koning RI, Svergun DI, Koster AJ, Fritzinger DC, Vogel CW, Gros P (2009) Insights into complement convertase formation based on the structure of the factor B-cobra venom factor complex. *EMBO J* 28: 2469 – 2478

Janssen BJ, Huizinga EG, Raaijmakers HC, Roos A, Daha MR, Nilsson-Ekdahl K, Nilsson B, Gros P (2005) Structures of complement component C3 provide insights into the function and evolution of immunity. *Nature* 437: 505 – 511

Jokiranta TS, Hellwage J, Koistinen V, Zipfel PF, Meri S (2000) Each of the three binding sites on complement factor H interacts with a distinct site on C3b. *J Biol Chem* 275: 27657 – 27662

Kabsch W (2010) Xds. *Acta Crystallogr D Biol Crystallogr* 66: 125 – 132

Kajander T, Lehtinen MJ, Hyvarinen S, Bhattacharjee A, Leung E, Isenman DE, Meri S, Goldman A, Jokiranta TS (2011) Dual interaction of factor H with C3d and glycosaminoglycans in host-nonhost discrimination by complement. *Proc Natl Acad Sci USA* 108: 2897 – 2902

Karplus PA, Diederichs K (2012) Linking crystallographic model and data quality. *Science* 336: 1030 – 1033

Katschke KJ Jr, Stawicki S, Yin J, Steffek M, Xi H, Sturgeon L, Hass PE, Loyet KM, Deforge L, Wu Y, van Lookeren Campagne M, Wiesmann C (2009) Structural and functional analysis of a C3b-specific antibody that selectively inhibits the alternative pathway of complement. *J Biol Chem* 284: 10473 – 10479

Kidmose RT, Laursen NS, Dobo J, Kjaer TR, Sirotkina S, Yatime L, Sottrup-Jensen L, Thiel S, Gal P, Andersen GR (2012) Structural basis for activation of the complement system by component C4 cleavage. *Proc Natl Acad Sci USA* 109: 15425 – 15430

Kirkitadze MD, Barlow PN (2001) Structure and flexibility of the multiple domain proteins that regulate complement activation. *Immunol Rev* 180: 146 – 161

Kirkitadze MD, Krych M, Uhrin D, Dryden DT, Smith BO, Cooper A, Wang X, Hauhart R, Atkinson JP, Barlow PN (1999) Independently melting modules and highly structured intermodular junctions within complement receptor type 1. *Biochemistry* 38: 7019 – 7031

Krissinel E, Henrick K (2007) Inference of macromolecular assemblies from crystalline state. *J Mol Biol* 372: 774 – 797

Krych M, Clemenza L, Howdeshell D, Hauhart R, Hourcade D, Atkinson JP (1994) Analysis of the functional domains of complement receptor type 1 (C3b/C4b receptor; CD35) by substitution mutagenesis. *J Biol Chem* 269: 13273 – 13278

Krych M, Hauhart R, Atkinson JP (1998) Structure-function analysis of the active sites of complement receptor type 1. *J Biol Chem* 273: 8623 – 8629

Krych M, Hourcade D, Atkinson JP (1991) Sites within the complement C3b/C4b receptor important for the specificity of ligand binding. *Proc Natl Acad Sci USA* 88: 4353 – 4357

Krych-Goldberg M, Hauhart RE, Porzukowiak T, Atkinson JP (2005) Synergy between two active sites of human complement receptor type 1 (CD35) in complement regulation: implications for the structure of the classical pathway C3 convertase and generation of more potent inhibitors. *J Immunol* 175: 4528 – 4535

Krych-Goldberg M, Hauhart RE, Subramanian VB, Yurcisin BM 2nd, Crimmins DL, Hourcade DE, Atkinson JP (1999) Decay accelerating activity of complement receptor type 1 (CD35). Two active sites are required for dissociating C5 convertases. *J Biol Chem* 274: 31160 – 31168

Kuttner-Kondo L, Hourcade DE, Anderson VE, Muqim N, Mitchell L, Soares DC, Barlow PN, Medof ME (2007) Structure-based mapping of DAF active site residues that accelerate the decay of C3 convertases. *J Biol Chem* 282: 18552 – 18562

Kuttner-Kondo LA, Dybvig MP, Mitchell LM, Muqim N, Atkinson JP, Medof ME, Hourcade DE (2003) A corresponding tyrosine residue in the C2/factor B type A domain is a hot spot in the decay acceleration of the complement C3 convertases. *J Biol Chem* 278: 52386 – 52391

Kuttner-Kondo LA, Mitchell L, Hourcade DE, Medof ME (2001) Characterization of the active sites in decay-accelerating factor. *J Immunol* 167: 2164 – 2171

Lambris JD, Lao Z, Oglesby TJ, Atkinson JP, Hack CE, Becherer JD (1996) Dissection of CR1, factor H, membrane cofactor protein, and factor B binding and functional sites in the third complement component. *J Immunol* 156: 4821 – 4832

Liszewski MK, Atkinson JP (2015a) Complement regulators in human disease: lessons from modern genetics. *J Intern Med* 277: 294 – 305

Liszewski MK, Atkinson JP (2015b) Complement regulator CD46: genetic variants and disease associations. *Hum Genomics* 9: 7

Liszewski MK, Leung M, Cui W, Subramanian VB, Parkinson J, Barlow PN, Manchester M, Atkinson JP (2000) Dissecting sites important for complement regulatory activity in membrane cofactor protein (MCP; CD46). *J Biol Chem* 275: 37692 – 37701

Liszewski MK, Leung MK, Atkinson JP (1998) Membrane cofactor protein: importance of N- and O-glycosylation for complement regulatory function. *J Immunol* 161: 3711 – 3718

Liszewski MK, Leung MK, Hauhart R, Buller RM, Bertram P, Wang X, Rosengard AM, Kotwal GJ, Atkinson JP (2006) Structure and regulatory profile of the monkeypox inhibitor of complement: comparison to homologs in vaccinia and variola and evidence for dimer formation. *J Immunol* 176: 3725 – 3734

Liszewski MK, Leung MK, Hauhart R, Fang CJ, Bertram P, Atkinson JP (2009) Smallpox inhibitor of complement enzymes (SPICE): dissecting functional sites and abrogating activity. *J Immunol* 183: 3150 – 3159

Lukacik P, Roversi P, White J, Esser D, Smith GP, Billington J, Williams PA, Rudd PM, Wormald MR, Harvey DJ, Crispin MD, Radcliffe CM, Dwek RA, Evans DJ, Morgan BP, Smith RA, Lea SM (2004) Complement regulation at the molecular level: the structure of decay-accelerating factor. *Proc Natl Acad Sci USA* 101: 1279 – 1284

Lutteke T, von der Lieth CW (2004) pdb-care (PDB carbohydrate residue check): a program to support annotation of complex carbohydrate structures in PDB files. *BMC Bioinformatics* 5: 69

Luzzatto L, Gianfaldoni G (2006) Recent advances in biological and clinical aspects of paroxysmal nocturnal hemoglobinuria. *Int J Hematol* 84: 104 – 112

Makou E, Herbert AP, Barlow PN (2013) Functional anatomy of complement factor H. *Biochemistry* 52: 3949 – 3962

Marrero A, Duquerroy S, Trapani S, Goulas T, Guevara T, Andersen GR, Navaza J, Sottrup-Jensen L, Gomis-Ruth FX (2012) The crystal structure of human alpha2-macroglobulin reveals a unique molecular cage. *Angew Chem Int Ed Engl* 51: 3340 – 3344

Martinez-Barricarte R, Heurich M, Lopez-Perrote A, Tortajada A, Pinto S, Lopez-Trascasa M, Sanchez-Corral P, Morgan BP, Llorca O, Harris CL, Rodriguez de Cordoba S (2015) The molecular and structural bases for the association of complement C3 mutations with atypical hemolytic uremic syndrome. *Mol Immunol* 66: 263 – 273

Martinez-Barricarte R, Heurich M, Valdes-Canedo F, Vazquez-Martul E, Torreira E, Montes T, Tortajada A, Pinto S, Lopez-Trascasa M, Morgan BP, Llorca O, Harris CL, Rodriguez de Cordoba S (2010) Human C3 mutation reveals a mechanism of dense deposit disease pathogenesis and provides insights into complement activation and regulation. *J Clin Invest* 120: 3702 – 3712

McCoy AJ, Grosse-Kunstleve RW, Adams PD, Winn MD, Storoni LC, Read RJ (2007) Phaser crystallographic software. *J Appl Crystallogr* 40: 658 – 674

McLure CA, Dawkins RL, Williamson JF, Davies RA, Berry J, Natalie LJ, Laird R, Gaudieri S (2004) Amino acid patterns within short consensus repeats define conserved duplicons shared by genes of the RCA complex. *J Mol Evol* 59: 143 – 157

Merle NS, Church SE, Fremeaux-Bacchi V, Roumenina LT (2015a) Complement System Part I - Molecular Mechanisms of Activation and Regulation. *Front Immunol* 6: 262

Merle NS, Noe R, Halbwachs-Mecarelli L, Fremeaux-Bacchi V, Roumenina LT (2015b) Complement System Part II: Role in Immunity. *Front Immunol* 6: 257

Morgan HP, Schmidt CQ, Guariento M, Blaum BS, Gillespie D, Herbert AP, Kavanagh D, Mertens HD, Svergun DI, Johansson CM, Uhrin D, Barlow PN, Hannan JP (2011) Structural basis for engagement by complement factor H of C3b on a self surface. *Nat Struct Mol Biol* 18: 463 – 470

Mortensen S, Kidmose RT, Petersen SV, Szilagyi A, Prohaszka Z, Andersen GR (2015) Structural Basis for the Function of Complement Component C4 within the Classical and Lectin Pathways of Complement. *J Immunol* 194: 5488 – 5496

Nicholson-Weller A, Wang CE (1994) Structure and function of decay accelerating factor CD55. *J Lab Clin Med* 123: 485 – 491

Nonaka M, Yoshizaki F (2004) Primitive complement system of invertebrates. *Immunol Rev* 198: 203 – 215

Noris M, Caprioli J, Bresin E, Mossali C, Pianetti G, Gamba S, Daina E, Fenili C, Castelletti F, Sorosina A, Piras R, Donadelli R, Maranta R, van der Meer I, Conway EM, Zipfel PF, Goodship TH, Remuzzi G (2010) Relative role of genetic complement abnormalities in sporadic and familial aHUS and their impact on clinical phenotype. *Clin J Am Soc Nephrol* 5: 1844 – 1859

Ojha H, Panwar HS, Gorham RD Jr, Morikis D, Sahu A (2014) Viral regulators of complement activation: structure, function and evolution. *Mol Immunol* 61: 89 – 99

Oran AE, Isenman DE (1999) Identification of residues within the 727–767 segment of human complement component C3 important for its interaction with factor H and with complement receptor 1 (CR1, CD35). *J Biol Chem* 274: 5120 – 5130

Park HJ, Guariento M, Maciejewski M, Hauhart R, Tham WH, Cowman AF, Schmidt CQ, Mertens HD, Liszewski MK, Hourcade DE, Barlow PN, Atkinson JP (2014) Using mutagenesis and structural biology to map the binding site for the Plasmodium falciparum merozoite protein PfRh4 on the human immune adherence receptor. *J Biol Chem* 289: 450 – 463

Pechtl IC, Kavanagh D, McIntosh N, Harris CL, Barlow PN (2011) Disease-associated N-terminal complement factor H mutations perturb cofactor and decay-accelerating activities. *J Biol Chem* 286: 11082 – 11090

Persson BD, Schmitz NB, Santiago C, Zocher G, Larvie M, Scheu U, Casasnovas JM, Stehle T (2010) Structure of the extracellular portion of CD46 provides insights into its interactions with complement proteins and pathogens. *PLoS Pathog* 6: e1001122

Reeves PJ, Callewaert N, Contreras R, Khorana HG (2002) Structure and function in rhodopsin: high-level expression of rhodopsin with restricted and homogeneous N-glycosylation by a tetracycline-inducible N-acetylglucosaminyltransferase I-negative HEK293S stable mammalian cell line. *Proc Natl Acad Sci USA* 99: 13419 – 13424

Richards A, Kemp EJ, Liszewski MK, Goodship JA, Lampe AK, Decorte R, Muslumanoglu MH, Kavukcu S, Filler G, Pirson Y, Wen LS, Atkinson JP, Goodship TH (2003) Mutations in human complement regulator, membrane cofactor protein (CD46), predispose to development of familial hemolytic uremic syndrome. *Proc Natl Acad Sci USA* 100: 12966 – 12971

Ricklin D, Hajishengallis G, Yang K, Lambris JD (2010) Complement: a key system for immune surveillance and homeostasis. *Nat Immunol* 11: 785 – 797

Ricklin D, Lambris JD (2013a) Complement in immune and inflammatory disorders: pathophysiological mechanisms. *J Immunol* 190: 3831 – 3838

Ricklin D, Lambris JD (2013b) Complement in immune and inflammatory disorders: therapeutic interventions. *J Immunol* 190: 3839 – 3847

Riley RC, Tannenbaum PL, Abbott DH, Atkinson JP (2002) Cutting edge: inhibiting measles virus infection but promoting reproduction: an explanation for splicing and tissue-specific expression of CD46. *J Immunol* 169: 5405 – 5409

Rodriguez E, Rallapalli PM, Osborne AJ, Perkins SJ (2014) New functional and structural insights from updated mutational databases for complement factor H, Factor I, membrane cofactor protein and C3. *Biosci Rep* 34: e00146

Rooijakkers SH, Wu J, Ruyken M, van Domselaar R, Planken KL, Tzekou A, Ricklin D, Lambris JD, Janssen BJ, van Strijp JA, Gros P (2009) Structural and functional implications of the alternative complement pathway C3 convertase stabilized by a staphylococcal inhibitor. *Nat Immunol* 10: 721 – 727

Rosengard AM, Liu Y, Nie Z, Jimenez R (2002) Variola virus immune evasion design: expression of a highly efficient inhibitor of human complement. *Proc Natl Acad Sci USA* 99: 8808 – 8813

Roversi P, Johnson S, Caesar JJ, McLean F, Leath KJ, Tsiftsoglou SA, Morgan BP, Harris CL, Sim RB, Lea SM (2011) Structural basis for complement factor I control and its disease-associated sequence polymorphisms. *Proc Natl Acad Sci USA* 108: 12839 – 12844

Schmidt CQ, Bai H, Lin Z, Risitano AM, Barlow PN, Ricklin D, Lambris JD (2013) Rational engineering of a minimized immune inhibitor with unique triple-targeting properties. *J Immunol* 190: 5712 – 5721

Schmidt CQ, Kennedy AT, Tham WH (2015) More than just immune evasion: Hijacking complement by Plasmodium falciparum. *Mol Immunol* 67: 71 – 84

Schramm EC, Roumenina LT, Rybkine T, Chauvet S, Vieira-Martins P, Hue C, Maga T, Valoti E, Wilson V, Jokiranta S, Smith RJ, Noris M, Goodship T, Atkinson JP, Fremeaux-Bacchi V (2015) Mapping interactions between complement C3 and regulators using mutations in atypical hemolytic uremic syndrome. *Blood* 125: 2359 – 2369

Sfyroera G, Katragadda M, Morikis D, Isaacs SN, Lambris JD (2005) Electrostatic modeling predicts the activities of orthopoxvirus complement control proteins. *J Immunol* 174: 2143 – 2151

Sjoberg AP, Trouw LA, Blom AM (2009) Complement activation and inhibition: a delicate balance. *Trends Immunol* 30: 83 – 90

Smith BO, Mallin RL, Krych-Goldberg M, Wang X, Hauhart RE, Bromek K, Uhrin D, Atkinson JP, Barlow PN (2002) Structure of the C3b binding site of CR1 (CD35), the immune adherence receptor. *Cell* 108: 769 – 780

Thomas BN, Donvito B, Cockburn I, Fandeur T, Rowe JA, Cohen JH, Moulds JM (2005) A complement receptor-1 polymorphism with high frequency in malaria endemic regions of Asia but not Africa. *Genes Immun* 6: 31 – 36

Till M, Robson A, Byrne MJ, Nair AV, Kolek SA, Shaw Stewart PD, Race PR (2013) Improving the success rate of protein crystallization by random microseed matrix screening. *J Vis Exp* 78: 50548

Tortajada A, Montes T, Martinez-Barricarte R, Morgan BP, Harris CL, de Cordoba SR (2009) The disease-protective complement factor H allotypic variant Ile62 shows increased binding affinity for C3b and enhanced cofactor activity. *Hum Mol Genet* 18: 3452 – 3461

Uhrinova S, Lin F, Ball G, Bromek K, Uhrin D, Medof ME, Barlow PN (2003) Solution structure of a functionally active fragment of decay-accelerating factor. *Proc Natl Acad Sci USA* 100: 4718 – 4723

Weisman HF, Bartow T, Leppo MK, Boyle MP, Marsh HC Jr, Carson GR, Roux KH, Weisfeldt ML, Fearon DT (1990) Recombinant soluble CR1 suppressed complement activation, inflammation, and necrosis associated with reperfusion of ischemic myocardium. *Trans Assoc Am Physicians* 103: 64 – 72

Wiesmann C, Katschke KJ, Yin J, Helmy KY, Steffek M, Fairbrother WJ, McCallum SA, Embuscado L, DeForge L, Hass PE, van Lookeren Campagne M (2006) Structure of C3b in complex with CRIg gives insights into regulation of complement activation. *Nature* 444: 217 – 220

Williams P, Chaudhry Y, Goodfellow IG, Billington J, Powell R, Spiller OB, Evans DJ, Lea S (2003) Mapping CD55 function. The structure of two pathogen-binding domains at 1.7 A. *J Biol Chem* 278: 10691 – 10696

Wu J, Wu YQ, Ricklin D, Janssen BJ, Lambris JD, Gros P (2009) Structure of complement fragment C3b-factor H and implications for host protection by complement regulators. *Nat Immunol* 10: 728 – 733

Yadav VN, Pyaram K, Mullick J, Sahu A (2008) Identification of hot spots in the variola virus complement inhibitor (SPICE) for human complement regulation. *J Virol* 82: 3283 – 3294

Zipfel PF, Hallstrom T, Riesbeck K (2013) Human complement control and complement evasion by pathogenic microbes–tipping the balance. *Mol Immunol* 56: 152 – 160

Zipfel PF, Skerka C (2009) Complement regulators and inhibitory proteins. *Nat Rev Immunol* 9: 729 – 740